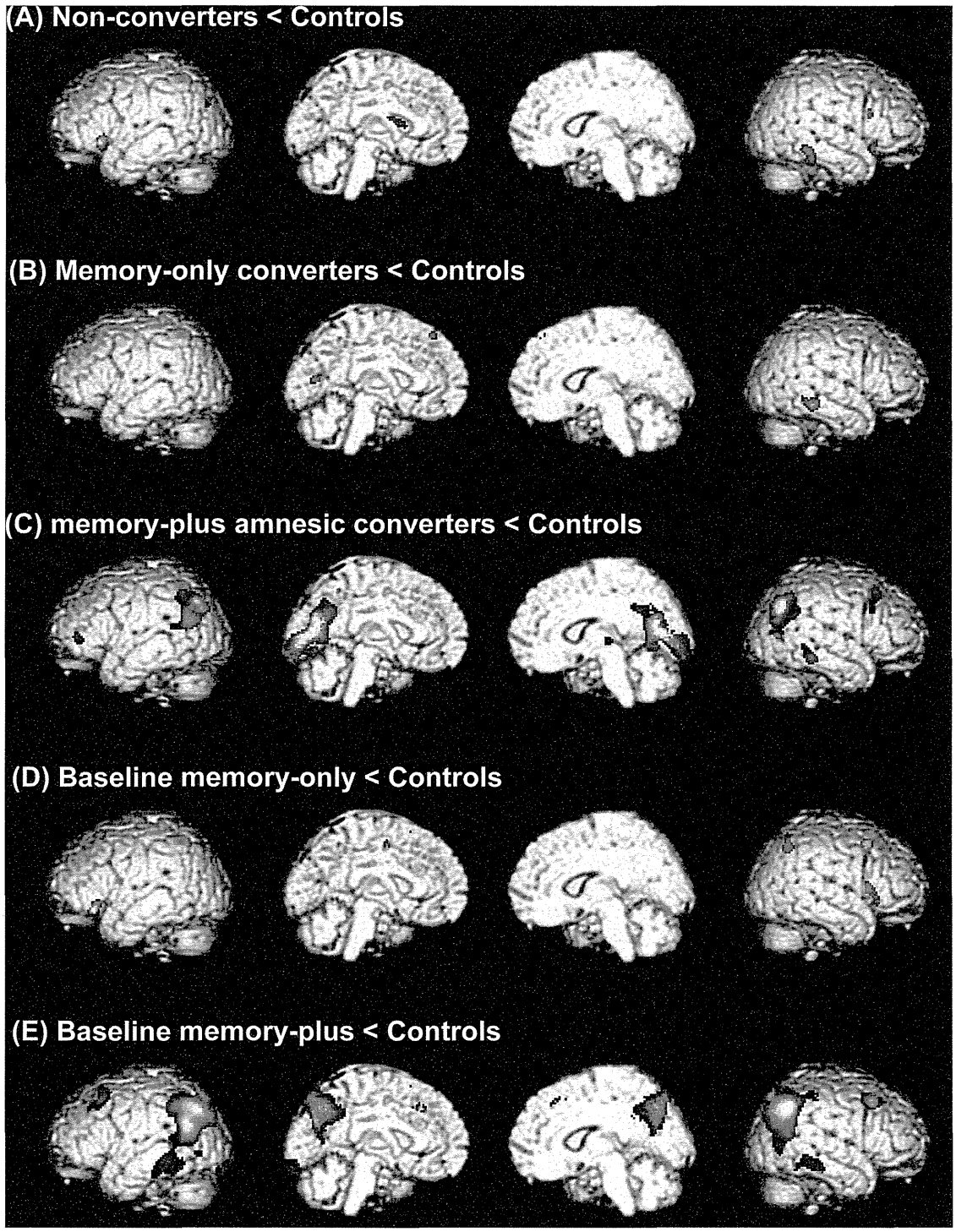

Figure 2. Areas of relative reduction in regional cerebral glucose metabolism in the patient groups compared with controls. Rendered images are shown in the order of the left lateral, left medial, right medial and right lateral.
doi:10.1371/journal.pone.0110547.g002

if the memory-plus converters represented a more advanced stage of the disease than did the other groups, they would not present with an equivalent severity of motor symptoms. Second, a comparison of metabolic patterns between the baseline memory-only and the baseline memory-plus patients showed a double dissociation in which posterior neocortical hypometabolism was more severe in the baseline memory-plus patients, whereas hypometabolism in the medial temporal lobe was more severe in the baseline memory-only patients (**Figures 3D and 3E**). These findings suggest that the brainstem and neocortex may be affected nearly simultaneously without marked limbic involvement in the memory-plus converters and the baseline memory-plus patients. A parallel finding was reported in a population-based cohort study in which incidental Lewy-related pathology was found in the

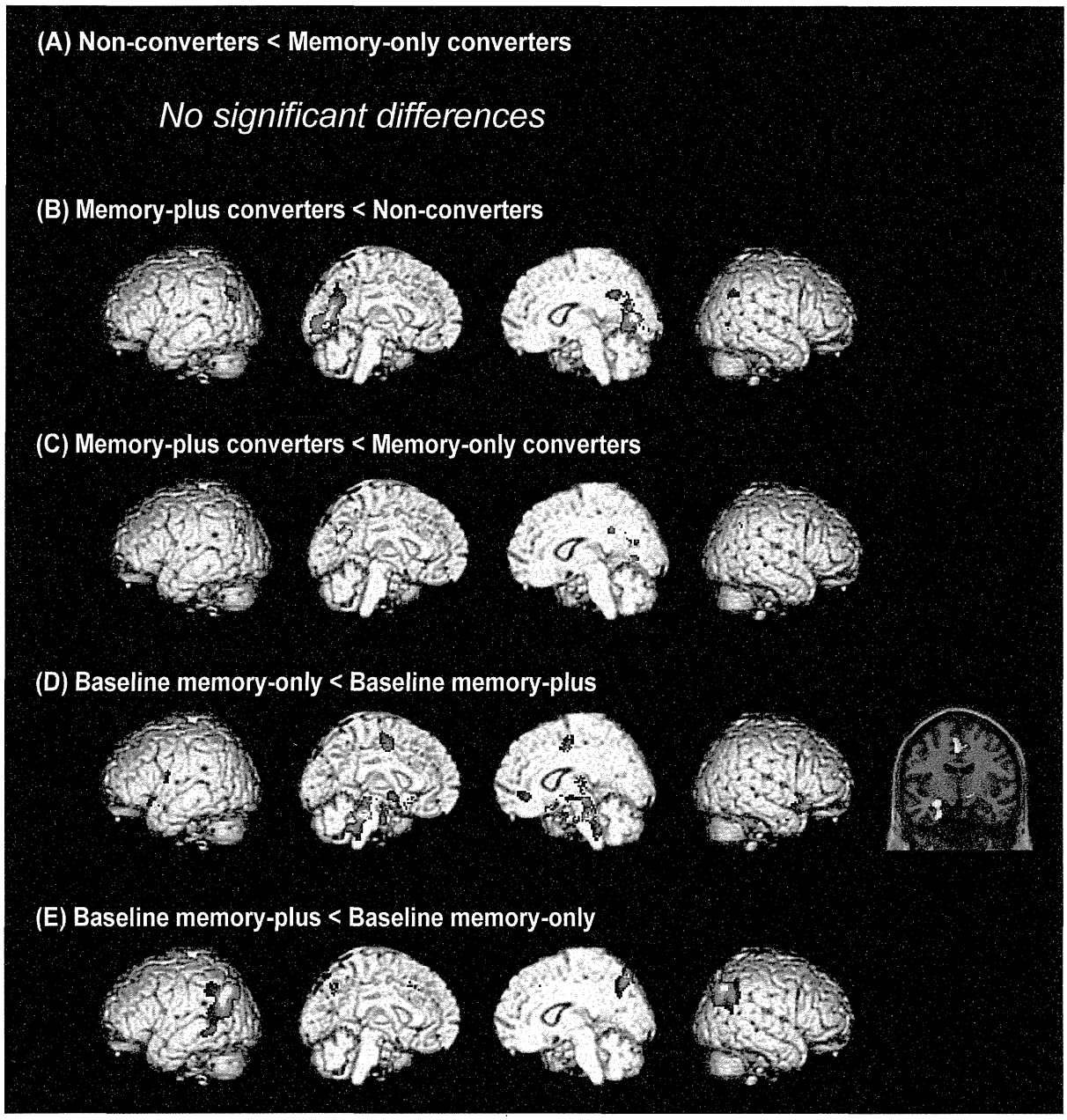

Figure 3. Group comparisons of regional cerebral glucose metabolism at baseline. (A) to (C) show the results of comparisons between patient groups with baseline Clinical Dementia Rating (CDR) 0, and (D) and (E) show the results of comparisons between groups with baseline CDR 0.5. Rendered images are shown in the order of the left lateral, left medial, right medial and right lateral. The left side of a coronal section corresponds to the left side of the brain.
doi:10.1371/journal.pone.0110547.g003

brainstem and neocortex but not in the limbic structures (medial temporal and cingulate cortices) in 3% of cases. [36].

From the viewpoint of prediction and early intervention, it is critical to establish the cognitive and neuroimaging features that are associated with rapid symptomatic deterioration and the future development of dementia. [2] In the current study, the memory-plus converters exhibited clinical features that are consistent with those of the clinical subtype associated with the rapid progression of motor symptoms and/or dementia, including rapid declines in the CDR sum of boxes and the UPDRS part III scores, and non-tremor dominant motor features (**Table 1**). [4,5,6] They had impaired performance on the overlapping-figure test (**Table 1**) and posterior cortical hypometabolism at baseline (**Figures 2C, 3B and 3C**), suggesting that early visuoperceptual impairment and posterior neocortical involvement may be risk factors for rapid symptomatic deterioration and the future development of dementia. The predictive value of visuoperceptual impairment for the future development of dementia in PD has been demonstrated in 3 of the 4 previous longitudinal neuropsychological studies with a follow-up of 2 years or more. [37,38,39,40] Similarly, a recent study demonstrated that patients with non-amnestic multi-domain MCI that had visuoperceptual deficits were associated with bradykinesia and gait disturbance (non-tremor-dominant motor features), suggesting a link to the rapidly progressive, dementia-

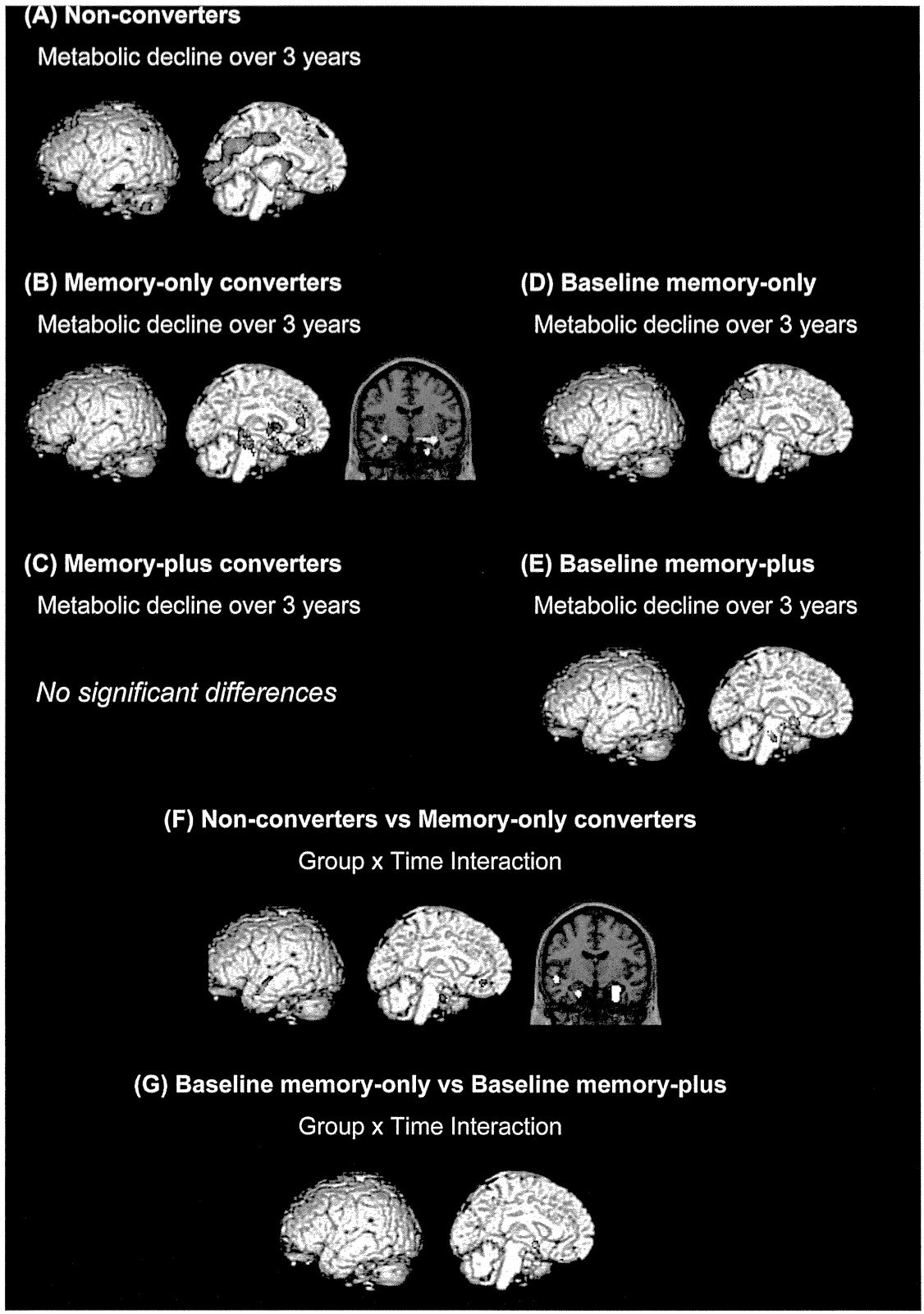

Figure 4. Longitudinal changes in regional cerebral glucose metabolism. (A) to (E) show 3-year metabolic declines in the individual patient groups. (F) and (G) show group x time interactions between the non-converters and the memory-only converters and between the baseline memory-only patients and the baseline memory-plus patients, respectively. Rendered images show the left hemisphere. The left sides of coronal sections correspond to the left side of the brain.
doi:10.1371/journal.pone.0110547.g004

related clinico-pathological subtype. [41] Although there is no neuropathological evidence for the relationship between lesions in the particular cortical regions and rapid symptomatic progression and dementia in PD, a previous longitudinal FDG-PET study demonstrated that parieto-occipital hypometabolism preceded the development of dementia. [42].

Memory impairment and its predictive value for future development of dementia in PD

Recent studies have demonstrated that memory impairment is the most common cognitive deficit in non-demented PD. [43,44] In agreement with these findings, positive scores on the memory subdomain were the most commonly observed CDR findings and baseline impairment in the ADAS-word recall test was found in 45% of the patients in the current study (**Tables 1 and 2**). However, the results of the previous longitudinal neuropsychological studies were split regarding the predictive value of memory impairment for dementia in PD. [37,38,39,40] One of the possible factors associated with this inconsistency is the variability of memory tests. The materials to be remembered (words, stories or figures) and the duration of retention (immediate or delayed) vary from test to test. Another possible factor which contribute to the low predictive value of memory impairment for dementia is the variability of the neural substrates of memory impairment in PD. Memory impairment in PD is associated with both dysexecutive retrieval deficits due to fronto-striatal dopaminergic insufficiency and mnemonic dysfunction due to hippocampal degeneration. [45] In the current study, baseline impairment on the backward digit-span observed in the memory-only converters suggests the possible contribution of executive/working memory deficits to memory complaints in PD (**Table 1**), whereas the relative medial temporal hypometabolism in the memory-only converters and the baseline memory-only patients suggested the role for hippocampal/medial temporal dysfunction (**Figures 3D, 4B and 4F**). Furthermore, a third mechanism of memory impairment is indicated by the findings of the current study; the memory-plus converters and the baseline memory-plus patients did not show significant hypometabolism in the medial temporal lobe despite their obvious memory problems, but they instead showed temporo-parietal and medial parietal hypometabolism (**Figures 2C, 2E, 3B, 3C and 3E**). The involvement of the parietal lobe in memory tasks has been documented in functional neuroimaging studies, but its functional role has been a matter of debate. [46].

Limitations

There are a number of limitations in the current study. First, although we claim that the memory-plus converters represent the rapidly progressive clinical subtype, no significant metabolic changes over 3 years were observed in this patient group. The following reasons can be suggested for this negative finding: (1) the small sample size may have result in a low statistical power; and (2) diffuse metabolic decline across the entire cerebral cortex may have obscured by the proportional scaling in the PET analysis. Consistent with the latter, a supplementary PET analysis in which a cerebellar reference was used instead of the proportional scaling demonstrated a CMRglc reduction over 3 years in the prefrontal cortex in the memory-plus converters (**Figure S1**).

Second, there were substantial inconsistencies between the CDR-based criteria and performance on the individual neuropsychological tests. Although patients with a CDR of 0 were defined as cognitively normal' according to our criteria, some were impaired in one or more neuropsychological tests. This inconsistency is most likely due to the insensitivity of the CDR to slight cognitive impairment, particularly in the executive and visuoperceptual domains. By contrast, neuropsychological tests failed to detect cognitive declines over time in the memory-only converters and memory-plus converters, despite the obvious cognitive deterioration documented by the CDR (**Table 1**). Measuring longitudinal cognitive changes using neuropsychological tests is contaminated by spurious improvement associated with practice effects. [20,21,22,23] Although the neuropsychological tests were administered twice with a relatively long interval of 3 years in the current study, previous studies demonstrated that practice effects persist over 5 years and are strongest between the first and second administrations. [20,47,48] Furthermore, the impact of dopaminergic therapy on cognition and mood should be taken into account in PD patients. A formal definitions of clinically meaningful cognitive decline' in PD should be established in future studies. [29] In addition, the criteria for at-risk state for dementia or PD-MCI should be not only sensitive but also specific. Insensitive criteria would lead to the oversight of at-risk patients of dementia, whereas an overly sensitive and insufficiently specific ones would make every PD patient an at-risk one because almost every PD patient is impaired in some of highly-demanded cognitive tasks.

Third, we separately analyzed the patient groups with a baseline CDR of 0 and those with a CDR of 0.5 and integrated the results obtained from these separate analyses to discuss long-term (more than 3 years) cognitive changes. Our findings and discussion should be examined by studies with longer follow-up periods.

Finally, the reduction in glucose metabolism may reflect not only neurodegeneration itself but also the remote effects of lesions in distant neural structures. In addition, because FDG-PET is unable to differentiate between Alzheimer's disease-related and Lewy-related pathologies, further studies utilizing amyloid-PET and other neuroimaging techniques are necessary to examine these issues.

Supporting Information

Figure S1 The results of a cerebellar-referenced PET analysis for the patient groups with baseline CDR 0 (non-converters, memory-only converters and memory-plus converters). A two-way repeated-measures ANOVA with variables of no interest of age, sex and UPDRS part III score was used. The statistical threshold was set at an uncorrected $p<0.001$ at the voxel level and at 20 voxels at the cluster level.
(TIF)

Author Contributions

Conceived and designed the experiments: YS YN TB EM. Performed the experiments: YN TB MU KY TI YH KH AT. Analyzed the data: YS YN. Contributed reagents/materials/analysis tools: HF MA TH EM. Contributed to the writing of the manuscript: YS YN.

References

1. Kehagia AA, Barker RA, Robbins TW (2010) Neuropsychological and clinical heterogeneity of cognitive impairment and dementia in patients with Parkinson's disease. Lancet Neurol 9: 1200–1213.

2. Litvan I, Aarsland D, Adler CH, Goldman JG, Kulisevsky J, et al. (2011) MDS Task Force on mild cognitive impairment in Parkinson's disease: critical review of PD-MCI. Mov Disord 26: 1814–1824.

3. Baba T, Kikuchi A, Hirayama K, Nishio Y, Hosokai Y, et al. (2012) Severe olfactory dysfunction is a prodromal symptom of dementia associated with Parkinson's disease: a 3 year longitudinal study. Brain 135: 161–169.
4. Burn DJ, Rowan EN, Allan LM, Molloy S, O'Brien JT, et al. (2006) Motor subtype and cognitive decline in Parkinson's disease, Parkinson's disease with dementia, and dementia with Lewy bodies. J Neurol Neurosurg Psychiatry 77: 585–589.
5. Lewis SJ, Foltynie T, Blackwell AD, Robbins TW, Owen AM, et al. (2005) Heterogeneity of Parkinson's disease in the early clinical stages using a data driven approach. J Neurol Neurosurg Psychiatry 76: 343–348.
6. van Rooden SM, Colas F, Martinez-Martin P, Visser M, Verbaan D, et al. (2011) Clinical subtypes of Parkinson's disease. Mov Disord 26: 51–58.
7. Halliday GM, Holton JL, Revesz T, Dickson DW (2011) Neuropathology underlying clinical variability in patients with synucleinopathies. Acta Neuropathol 122: 187–204.
8. Burton EJ, McKeith IG, Burn DJ, Williams ED, O'Brien JT (2004) Cerebral atrophy in Parkinson's disease with and without dementia: a comparison with Alzheimer's disease, dementia with Lewy bodies and controls. Brain 127: 791–800.
9. Hosokai Y, Nishio Y, Hirayama K, Takeda A, Ishioka T, et al. (2009) Distinct patterns of regional cerebral glucose metabolism in Parkinson's disease with and without mild cognitive impairment. Mov Disord 24: 854–862.
10. Huang C, Mattis P, Tang C, Perrine K, Carbon M, et al. (2007) Metabolic brain networks associated with cognitive function in Parkinson's disease. Neuroimage 34: 714–723.
11. Nagano-Saito A, Washimi Y, Arahata Y, Kachi T, Lerch JP, et al. (2005) Cerebral atrophy and its relation to cognitive impairment in Parkinson disease. Neurology 64: 224–229.
12. Summerfield C, Junque C, Tolosa E, Salgado-Pineda P, Gomez-Anson B, et al. (2005) Structural brain changes in Parkinson disease with dementia: a voxel-based morphometry study. Arch Neurol 62: 281–285.
13. Aarsland D, Perry R, Brown A, Larsen JP, Ballard C (2005) Neuropathology of dementia in Parkinson's disease: a prospective, community-based study. Ann Neurol 58: 773–776.
14. Compta Y, Parkkinen L, O'Sullivan SS, Vandrovcova J, Holton JL, et al. (2011) Lewy- and Alzheimer-type pathologies in Parkinson's disease dementia: which is more important? Brain 134: 1493–1505.
15. Selikhova M, Williams DR, Kempster PA, Holton JL, Revesz T, et al. (2009) A clinico-pathological study of subtypes in Parkinson's disease. Brain 132: 2947–2957.
16. Bohnen NI, Muller ML (2013) In vivo neurochemical imaging of olfactory dysfunction in Parkinson's disease. J Neural Transm 120: 571–576.
17. Nishio Y, Hirayama K, Takeda A, Hosokai Y, Ishioka T, et al. (2010) Corticolimbic gray matter loss in Parkinson's disease without dementia. Eur J Neurol 17: 1090–1097.
18. Amrerical Psychiatric Association. (1987) Diagnostic and Statistical Manual of Mental Disorders. 3rd, revised.
19. Morris JC (1997) Clinical dementia rating: a reliable and valid diagnostic and staging measure for dementia of the Alzheimer type. Int Psychogeriatr 9 Suppl 1: 173–176; discussion 177–178.
20. Abner EL, Dennis BC, Mathews MJ, Mendiondo MS, Caban-Holt A, et al. (2012) Practice effects in a longitudinal, multi-center Alzheimer's disease prevention clinical trial. Trials 13: 217.
21. Duff K, Beglinger LJ, Schultz SK, Moser DJ, McCaffrey RJ, et al. (2007) Practice effects in the prediction of long-term cognitive outcome in three patient samples: a novel prognostic index. Arch Clin Neuropsychol 22: 15–24.
22. Machulda MM, Pankratz VS, Christianson TJ, Ivnik RJ, Mielke MM, et al. (2013) Practice Effects and Longitudinal Cognitive Change in Normal Aging vs. Incident Mild Cognitive Impairment and Dementia in The Mayo Clinic Study of Aging. Clin Neuropsychol 27: 1247–1264.
23. Mathews M, Abner E, Caban-Holt A, Kryscio R, Schmitt F (2013) CERAD practice effects and attrition bias in a dementia prevention trial. Int Psychogeriatr 25: 1115–1123.
24. Mathews M, Abner E, Kryscio R, Jicha G, Cooper G, et al. (2014) Diagnostic accuracy and practice effects in the National Alzheimer's Coordinating Center Uniform Data Set neuropsychological battery. Alzheimers Dement. doi: 10.1016/j.jalz.2013.11.007.
25. Doody RS, Ferris SH, Salloway S, Sun Y, Goldman R, et al. (2009) Donepezil treatment of patients with MCI: a 48-week randomized, placebo-controlled trial. Neurology 72: 1555–1561.
26. Dubois B, Tolosa E, Katzenschlager R, Emre M, Lees AJ, et al. (2012) Donepezil in Parkinson's disease dementia: a randomized, double-blind efficacy and safety study. Mov Disord 27: 1230–1238.
27. Mori E, Ikeda M, Kosaka K (2012) Donepezil for dementia with Lewy bodies: a randomized, placebo-controlled trial. Ann Neurol 72: 41–52.
28. Rogers SL (1998) Perspectives in the management of Alzheimer's disease: clinical profile of donepezil. Dement Geriatr Cogn Disord 9 Suppl 3: 29–42.
29. Litvan I, Goldman JG, Troster AI, Schmand BA, Weintraub D, et al. (2012) Diagnostic criteria for mild cognitive impairment in Parkinson's disease: Movement Disorder Society Task Force guidelines. Mov Disord 27: 349–356.
30. Folstein MF, Robins LN, Helzer JE (1983) The Mini-Mental State Examination. Arch Gen Psychiatry 40: 812.
31. Mohs RC, Rosen WG, Davis KL (1983) The Alzheimer's disease assessment scale: an instrument for assessing treatment efficacy. Psychopharmacol Bull 19: 448–450.
32. Ishioka T, Hirayama K, Hosokai Y, Takeda A, Suzuki K, et al. (2011) Illusory misidentifications and cortical hypometabolism in Parkinson's disease. Mov Disord 26: 837–843.
33. Schrag A, Dodel R, Spottke A, Bornschein B, Siebert U, et al. (2007) Rate of clinical progression in Parkinson's disease. A prospective study. Mov Disord 22: 938–945.
34. Reijnders JS, Ehrt U, Lousberg R, Aarsland D, Leentjens AF (2009) The association between motor subtypes and psychopathology in Parkinson's disease. Parkinsonism Relat Disord 15: 379–382.
35. Braak H, Del Tredici K, Rub U, de Vos RA, Jansen Steur EN, et al. (2003) Staging of brain pathology related to sporadic Parkinson's disease. Neurobiol Aging 24: 197–211.
36. Zaccai J, Brayne C, McKeith I, Matthews F, Ince PG (2008) Patterns and stages of alpha-synucleinopathy: Relevance in a population-based cohort. Neurology 70: 1042–1048.
37. Janvin CC, Larsen JP, Aarsland D, Hugdahl K (2006) Subtypes of mild cognitive impairment in Parkinson's disease: progression to dementia. Mov Disord 21: 1343–1349.
38. Levy G, Jacobs DM, Tang MX, Cote LJ, Louis ED, et al. (2002) Memory and executive function impairment predict dementia in Parkinson's disease. Mov Disord 17: 1221–1226.
39. Mahieux F, Fenelon G, Flahault A, Manifacier MJ, Michelet D, et al. (1998) Neuropsychological prediction of dementia in Parkinson's disease. J Neurol Neurosurg Psychiatry 64: 178–183.
40. Williams-Gray CH, Foltynie T, Brayne CE, Robbins TW, Barker RA (2007) Evolution of cognitive dysfunction in an incident Parkinson's disease cohort. Brain 130: 1787–1798.
41. Goldman JG, Weis H, Stebbins G, Bernard B, Goetz CG (2012) Clinical differences among mild cognitive impairment subtypes in Parkinson's disease. Mov Disord 27: 1129–1136.
42. Bohnen NI, Koeppe RA, Minoshima S, Giordani B, Albin RL, et al. (2011) Cerebral glucose metabolic features of Parkinson disease and incident dementia: longitudinal study. J Nucl Med 52: 848–855.
43. Aarsland D, Bronnick K, Williams-Gray C, Weintraub D, Marder K, et al. (2010) Mild cognitive impairment in Parkinson disease: a multicenter pooled analysis. Neurology 75: 1062–1069.
44. Hanna-Pladdy B, Jones K, Cabanban R, Pahwa R, Lyons KE (2013) Predictors of mild cognitive impairment in early-stage Parkinson's disease. Dement Geriatr Cogn Dis Extra 3: 168–178.
45. Aarsland D, Bronnick K, Fladby T (2011) Mild cognitive impairment in Parkinson's disease. Curr Neurol Neurosci Rep 11: 371–378.
46. Wagner AD, Shannon BJ, Kahn I, Buckner RL (2005) Parietal lobe contributions to episodic memory retrieval. Trends Cogn Sci 9: 445–453.
47. Rabbitt P, Lunn M, Ibrahim S, McInnes L (2009) Further analyses of the effects of practice, dropout, sex, socio-economic advantage, and recruitment cohort differences during the University of Manchester longitudinal study of cognitive change in old age. Q J Exp Psychol (Hove) 62: 1859–1872.
48. Rabbitt P, Lunn M, Wong D, Cobain M (2008) Age and ability affect practice gains in longitudinal studies of cognitive change. J Gerontol B Psychol Sci Soc Sci 63: P235–P240.
49. Abe N, Fujii T, Hirayama K, Takeda A, Hosokai Y, et al. (2009) Do parkinsonian patients have trouble telling lies? The neurobiological basis of deceptive behaviour. Brain 132: 1386–1395.

Neurobiology of Disease 71 (2014) 1–13

Contents lists available at ScienceDirect

Neurobiology of Disease

journal homepage: www.elsevier.com/locate/ynbdi

VPS35 dysfunction impairs lysosomal degradation of α-synuclein and exacerbates neurotoxicity in a *Drosophila* model of Parkinson's disease

Emiko Miura [a,1], Takafumi Hasegawa [a,1,*], Masatoshi Konno [a,b,1], Mari Suzuki [b], Naoto Sugeno [a], Nobuhiro Fujikake [b], Sven Geisler [c], Mitsuaki Tabuchi [d], Ryuji Oshima [a], Akio Kikuchi [a], Toru Baba [a], Keiji Wada [b], Yoshitaka Nagai [b], Atsushi Takeda [a,e], Masashi Aoki [a]

[a] *Division of Neurology, Department of Neuroscience & Sensory Organs, Tohoku University Graduate School of Medicine, Sendai 980-8574, Japan*
[b] *Department of Degenerative Neurological Diseases, National Institute of Neuroscience, National Center of Neurology and Psychiatry (NCNP), Kodaira 187-8502, Japan*
[c] *Laboratory of Functional Neurogenetics, Department for Neurodegenerative Diseases, Hertie Institute for Clinical Brain Research, University of Tübingen, German Centre for Neurodegenerative Diseases (DZNE), 72076 Tübingen, Germany*
[d] *Laboratory of Applied Molecular Cell Biology, Faculty of Agriculture, Kagawa University, Kagawa 761-0795, Japan*
[e] *Department of Neurology, National Hospital Organization Sendai-Nishitaga Hospital, Sendai 982-8555, Japan*

ARTICLE INFO

Article history:
Received 3 May 2014
Revised 7 July 2014
Accepted 28 July 2014
Available online 6 August 2014

Keywords:
Parkinson's disease
VPS35
α-Synuclein
Retromer
Cathepsin D
Lysosome
Vesicular transport

ABSTRACT

Mutations in *vacuolar protein sorting 35* (*VPS35*) have been linked to familial Parkinson's disease (PD). VPS35, a component of the retromer, mediates the retrograde transport of cargo from the endosome to the trans-Golgi network. Here we showed that retromer depletion increases the lysosomal turnover of the mannose 6-phosphate receptor, thereby affecting the trafficking of cathepsin D (CTSD), a lysosome protease involved in α-synuclein (αSYN) degradation. VPS35 knockdown perturbed the maturation step of CTSD in parallel with the accumulation of αSYN in the lysosomes. Furthermore, we found that the knockdown of *Drosophila VPS35* not only induced the accumulation of the detergent-insoluble αSYN species in the brain but also exacerbated both locomotor impairments and mild compound eye disorganization and interommatidial bristle loss in flies expressing human αSYN. These findings indicate that the retromer may play a crucial role in αSYN degradation by modulating the maturation of CTSD and might thereby contribute to the pathogenesis of the disease.

Introduction

Parkinson's disease (PD), the second most common neurodegenerative disease, is clinically characterized by a progressive increase in movement disability, impaired balance, and a variety of nonmotor symptoms (Poewe and Mahlknecht, 2009). The pathological hallmark of PD is the loss of pigmented dopaminergic neurons in the substantia nigra pars compacta and the presence of Lewy bodies, which are composed primarily of α-synuclein (αSYN) fibrils (Spillantini et al., 1997). During the assembly of αSYN fibrils, various intermediate-state oligomers are formed, and these oligomers are suspected to be the main toxic species (Wales et al., 2013). The mechanisms underlying the selective neuronal loss in PD remain elusive; however, numerous etiopathogenic hypotheses have been proposed related to oxidative stress, endoplasmic reticulum stress, mitochondrial dysfunction, ubiquitin–proteasome dysfunction, and an impaired autophagy–lysosome pathway (Dehay et al., 2013; Hasegawa et al., 2006; Singleton et al., 2013; Springer and Kahle, 2011; Sugeno et al., 2008; Tofaris, 2012). Although more than 90% of PD cases occur sporadically, the identification of several genes linked to familial PD has offered great insight into the biochemical and molecular mechanisms of the disease. Recently, a missense mutation (p.D620N) in the *vacuolar protein sorting 35* (*VPS35*) gene was identified as the cause of an autosomal dominant form of PD (Vilarino-Guell et al., 2011; Zimprich et al., 2011). VPS35, a vital element of the retromer complex, mediates the retrograde

Abbreviations: Ab, antibody; AD, Alzheimer's disease; αSYN, α-synuclein; CTSD, cathepsin D; CI-MPR, cation-independent mannose 6-phosphate receptor; DMEM, Dulbecco's modified Eagle's medium; elav, embryonic lethal abnormal vision; FBS, fetal bovine serum; GMR, glass multiple reporter; HMW, high-molecular-weight; HRP, horseradish peroxidase; HSP, heat shock protein; LAMP, lysosome-associated membrane protein; M6P, mannose 6-phosphate; MTT, 3-(4,5-dimethylthiazo-2-yl)-2,5-diphenyltetrazolium bromide; NAB, N-aryl benzimidazole; Nedd4, neural precursor cell expressed developmentally down-regulated protein 4; PD, Parkinson's disease; PVDF, polyvinylidene difluoride; RFU, relative fluorescence unit; RIPA, radio-immunoprecipitation assay; RNAi, RNA interference; rp49, ribosomal protein 49; siRNA, small interfering RNA; SDS, sodium dodecyl sulfate; SNX, sorting nexin; TCA, trichloroacetic acid; Tg, transgenic; TGN, trans-Golgi network; UAS, upstream activating sequence; VPS35, vacuolar protein sorting 35; WASH, Wiskott–Aldrich syndrome protein and SCAR homolog; wt, wild-type.

* Corresponding author at: Division of Neurology, Department of Neuroscience & Sensory Organs, Tohoku University Graduate School of Medicine, 1-1, Seiryomachi, Aobaku, Sendai, Miyagi 980-8574, Japan. Fax: +81 22 717 7192.
E-mail address: thasegawa@med.tohoku.ac.jp (T. Hasegawa).

Available online on ScienceDirect (www.sciencedirect.com).

[1] These authors contributed equally to this study.

http://dx.doi.org/10.1016/j.nbd.2014.07.014
0969-9961/

transport of cargo from the endosome to the *trans*-Golgi network (TGN) (Seaman et al., 1997). Structurally, the retromer comprises two distinct subcomplexes: a cargo-recognition VPS26–VPS29–VPS35 heterotrimer and a membrane-targeting dimer of the sorting nexin (SNX1 and/or SNX2) (Hierro et al., 2007). One of the best-characterized types of cargo for the retromer is the cation-independent mannose 6-phosphate receptor (CI-MPR), which participates in the delivery of lysosomal enzymes, such as the aspartyl protease cathepsin D (CTSD), to lysosomes (Seaman, 2004). Upon arrival in the Golgi apparatus, newly synthesized lysosomal enzymes are specifically modified with mannose 6-phosphate (M6P) residues, which are recognized by the CI-MPR in the TGN. Under physiological conditions, newly synthesized CTSD binds CI-MPR in the TGN and is translocated into endosomes; the CTSD is then released for further transport to lysosomes. The retromer retrieves the unoccupied MPRs from endosomes and relocates them to the TGN, where they participate in further cycles of CTSD sorting. Because CTSD is the main lysosomal endopeptidase responsible for the degradation of long-lived proteins, including αSYN (Cullen et al., 2009; Sevlever et al., 2008), it is tempting to speculate that a VPS35 malfunction may decrease the active form of CTSD in lysosomes and thus lead to an abnormal αSYN accumulation.

To further clarify the pathophysiological roles of the retromer in αSYN catabolism, RNA interference (RNAi)-mediated silencing of *VPS35* was performed using cellular and *in vivo* human wild-type (wt) αSYN (*h[wt]-SNCA*)-expressing transgenic fly models. In this study, we found that interference with the retromer function resulted in the aberrant maturation of CTSD, which led to the accumulation of intracellular αSYN, mainly in the late endosome/lysosome compartments. Furthermore, we showed that the knockdown of *Drosophila melanogaster VPS35* (*dVPS35*) exacerbated the locomotor abnormalities and mild compound eye disorganization and interommatidial bristle loss in human αSYN transgenic (Tg) flies. Our study provides evidence that the retromer may play a critical role in αSYN catabolism and thus drive the pathogenic process in synucleinopathies.

Materials and methods

Cell culture and plasmid transfection

HEK293 cells were maintained in Dulbecco's modified Eagle's medium (DMEM) with high glucose (4500 mg/L; Life Technologies/GIBCO, Carlsbad, CA) supplemented with L-glutamine and 10% fetal bovine serum (FBS; Thermo Scientific/HyClone, Rockford, IL). Plasmids (5 μg DNA for 1×10^6 cells) were introduced into these cells using the NEPA21® square wave electroporator according to the manufacturer's protocol (NEPA Gene, Chiba, Japan). Electroporation parameters consisted of a poring pulse (115 V, 7.5 ms in length with 50 ms interval) and a transfer pulse (20 V, 50 ms in length with 50 ms interval). For the stable transfection of HA-tagged and untagged αSYN in HEK293 cells, transfected cells were maintained under selective pressure with 800 μg/ml of G418 (InvivoGen, San Diego, CA).

Plasmid construction and preparation

Human CTSD cDNA (NM_001909.4) was subcloned into a pCMV vector. The cDNA encoding h[wt]-SNCA (NM_000345.3) with a Kozak consensus sequence was introduced into pcDNA3.1 + and 2xHA pRc/CMV vectors (RIKEN Bioresource Center, Tsukuba, Japan). Human wt and mutant (D620N and P316S) VPS35 cDNAs (GenBank AF175265.1) were subcloned into a pcDNA6.2/N-V5 vector (Life Technologies). Plasmid DNAs were isolated and purified using the GenoPure Plasmid Maxi Kit (Roche, Indianapolis, IN). The fidelity and orientation of the expression constructs were confirmed by restriction digestion and direct nucleotide sequencing.

RNA interference

The following small interfering RNAs (siRNAs) were used to ablate the expression of human VPS35: *VPS35* siRNA#1, 5′-GCCUUCAGAGGAUGUUGUAUCUUUA-3′ and *VPS35* siRNA#2, 5′-GCAUGAGUUGUUAUGUGCUUAGUAA-3′ (Stealth™ siRNA duplex oligoribonucleotides, Life Technologies/Invitrogen). Scrambled control siRNA (sc-36869) was purchased from Santa Cruz Biotechnology (Santa Cruz, CA). HEK293 cells were transfected with the target-specific or control scrambled siRNA (2 μg siRNA for 1×10^6 cells) using a NEPA21 square wave electroporator according to the manufacturer's protocol. Electroporation parameters included a poring pulse (115 V, 7.5 ms in length with 50 ms intervals) and a transfer pulse (20 V, 50 ms in length with 50 ms intervals). Thirty-three hours after the gene silencing, the cells were harvested and subjected to further studies. To evaluate the degradation kinetics of αSYN by CTSD, human CTSD was expressed for 24 h in HEK293 cells stably expressing αSYN. The cells were then treated with cycloheximide (0.1 μg/μl, purchased from Sigma) for 24 h. Chloroquine diphosphate (Sigma; 50 μM for 5 h) was used to examine the role of lysosomal function on αSYN degradation.

Subcellular fractionation

Subcellular fractionation was performed according to methods described previously (Hasegawa et al., 2011). In brief, mechanically harvested cells (1×10^8) were resuspended in 2 ml ice-cold fractionation buffer (10 mM Tris/acetic acid pH 7.0 and 250 mM sucrose) and homogenized using 20 strokes in a 2-ml Dounce tissue grinder with a tight pestle (GPE, Bedfordshire, England). The homogenate was cleared by three successive centrifugation steps (500 ×*g* for 2 min, 1000 ×*g* for 2 min and 2000 ×*g* for 2 min). The supernatant was centrifuged at 4000 ×*g* for 2 min to pellet the plasma membrane and nuclei. The supernatant was then ultracentrifuged at 100,000 ×*g* (P50S2 swing rotor, Hitachi Koki Co., Ltd., Tokyo, Japan) for 2 min to pellet the mitochondria, endosomes, and lysosomes (fraction EL). Lysosomes were isolated from the fraction EL by a 10-min osmotic lysis using 5 times the pellet volume of distilled water. After another centrifugation step at 100,000 ×*g* for 2 min, the lysosomes remained in the supernatant, whereas the endosomes and mitochondria were in the pellet.

Protein extraction from culture medium

Protein in the medium was extracted using a trichloroacetic acid (TCA)/acetone precipitation (Hasegawa et al., 2011). In brief, the culture medium was cleared by three successive centrifugation steps (800 ×*g* for 5 min, 2000 ×*g* for 10 min, and 10,000 ×*g* for 20 min at 4 °C). The supernatant was transferred to a new tube, and an equal volume of ice-cold 20% TCA/acetone was added, followed by incubation at −20 °C for 3 h. After adding 3 volumes of acetone, the protein was allowed to precipitate overnight at −20 °C. The protein was pelleted by centrifugation at 5000 ×*g* for 60 min, dissolved in 8 M urea/5% SDS with sonication, and subjected to Western blotting.

Cathepsin D activity assay

The bioactivity of CTSD in cultured cells was measured by a fluorescence-based assay using MCA-GKPILFFRLK(DNP)-dR-NH_2 as a synthetic substrate (CTSD Activity Assay Kit; BioVision, Mountain View, CA). Fluorescence was measured at an excitation/emission = 328/460 nm using a Varioskan Flash microplate reader (Thermo Scientific, Asheville, NC). The specific enzymatic activity was calculated as the relative fluorescence unit divided by the total protein concentration (relative fluorescence unit; RFU/μg protein). Pooled data from 5 independent experiments were statistically analyzed using one-way ANOVA with a post-hoc Dunnett's test using GraphPad Prism version 6 for Mac OS X (GraphPad Software, CA).

Western immunoblot analysis

After preparing the cell lysates using radio-immunoprecipitation assay (RIPA) buffer (1% NP-40, 0.5% deoxycholate, 0.1% sodium dodecyl sulfate (SDS), 1 mM EDTA, 10 m M sodium pyrophosphate, 50 mM sodium fluoride, 1 mM sodium orthovanadate, 150 mM sodium chloride, 50 mM Tris–HCl (pH 8.0) plus 1× Cømplete protease inhibitor cocktail; Roche), the protein concentration was determined using a BCA protein assay kit (BioRad, Hercules, CA). The lysate (15 μg) was electrophoresed on SDS-PAGE gels and transferred onto polyvinylidene difluoride (PVDF) membranes using the Trans-Blot Turbo® transfer system (BioRad). For the detection of human αSYN in the fly brain, five dissected fly heads were homogenized in Triton lysis buffer (50 mM Tris–HCl (pH 7.4), 1% Triton X-100, 150 mM NaCl, 1 mM EDTA plus protease inhibitors) using a Biomasher II® tissue grinder (Nippi Inc., Tokyo, Japan). After centrifugation at 15,000 ×*g* for 20 min, the supernatant was collected as the Triton-soluble fraction. The remaining pellet was further dissolved into a 2× Laemmli buffer with sonication and was centrifuged at 15,000 ×*g* for 20 min. The supernatant was collected as the Triton-insoluble fraction. For improved detection of αSYN in fly brain, transferred PVDF membranes were soaked in 0.4% paraformaldehyde/PBS for 30 min prior to the blocking step (Lee and Kamitani, 2011). After blocking with 5% milk in Tris-buffered saline with 0.1% Tween 20, the membranes were incubated with the following antibodies (Abs); anti-VPS35 ([C3], C-term Ab, 1:2000; GeneTex, Irvine, CA), anti-CTSD (clone C-20, 1:2000; Santa Cruz), anti-CI-MPR (#5230-1, 1:20,000; Epitomics, Burlingame, CA), anti-VPS26 (ab23892, 1:4000; Abcam, Cambridge, UK), anti-VPS29 (H00051699-A01, 1:500; Abnova, Taipei, Taiwan), anti-α-tubulin (clone DM1A, 1:1000; Sigma, St. Louis, MO), anti-syn-1 (610787, 1:1000; BD Bioscience, San Jose, CA), anti-HA-tag (clone 6E2, 1:1000; CST, Danvers, MA), anti-V5-tag (R960-25, 1:1000; Invitrogen), anti-albumin (#4929, 1:4000; CST), anti-Rab5 (clone S-19, 1:2000; Santa Cruz), anti-LAMP-2 (clone H4B4, 1:1000; DSHB, Iowa City, IA) and anti-Hsp90 (SPA-846, 1:4000; Stressgen, Victoria, BC, Canada). Primary Abs were followed by incubation with HRP-conjugated secondary Abs (1:10000; Jackson ImmunoResearch Laboratories, West Grove, PA). Bands were visualized with Luminata Forte HRP Substrate (Millipore, Bedford, MA) and images were captured by an Omega Lum G™ image analyzer (Aplegen, Pleasanton, CA). Quantification of the band intensity was performed using Image J software (NIH, Bethesda, MD). Pooled data from four independent experiments were statistically analyzed by a one-way ANOVA or unpaired Student's *t*-test.

Coimmunoprecipitation

Coimmunoprecipitation was performed according to the method described previously (Hasegawa et al., 2010). In brief, 48 h post-transfection, HEK293 cells were lysed in TNE buffer containing 50 mM Tris–HCl (pH 7.4), 150 mM NaCl, 0.5% NP-40, 1 mM EDTA and 1× protease inhibitor cocktail (Roche). Lysate containing 500 μg of protein was immunoprecipitated with 3 μl of V5 Ab (Life Technologies/Invitrogen) overnight on a carousel at 4 °C. Immune complexes were allowed to bind to Protein A/G PLUS-Agarose (Santa Cruz) for 2 h at 4 °C. After washing 5 times with TNE buffer containing 0.1% NP-40, protein complexes were eluted with 2× non-reducing Laemmli buffer and subsequently analyzed by Western blotting.

Immunofluorescence confocal microscopy

Immunostaining was performed according to methods previously described (Hasegawa et al., 2010). The primary Abs used included anti-VPS35 (GeneTex) and anti-CI-MPR (Epitomics) Abs. Positive immunostainings were detected using Alexa 488- and Alexa 568-conjugated secondary Abs (Molecular Probes/Life Technologies). Nuclei were counterstained with the far-red fluorescent DNA dye DRAQ7™ (CST) and were pseudocolored blue. Images were analyzed with a FluoView FV300 confocal laser microscope system equipped with HeNe-Green (543 nm), HeNe-Red (633 nm) and Ar (488 nm) laser units (Olympus, Tokyo, Japan). In multi-labeling experiments, images were collected using a single excitation for each wavelength separately, and were then merged using Fluoview image analysis software (version 4.1, Olympus).

Drosophila stocks

Fly culture and crosses were performed under standard conditions at 25 °C. The fly lines bearing *elav*-GAL4, *Act5c*-GAL4, *UAS*-EGFP, *UAS*-GFP dsRNA (*GFP*-RNAi), and *UAS-h[wt]-SNCA* transgenes were obtained from the Bloomington *Drosophila* Stock Center at Indiana University (BDSC, Bloomington, IN). The *VPS35* RNAi fly lines (#45570 and #22180, designated as *dVPS35* RNAi-1 and *dVPS35* RNAi-2, respectively) were provided by the Vienna Drosophila RNAi Center (VDRC, Vienna, Austria). Tg fly lines bearing the *GMR*-GAL4 have been described previously (Yamaguchi et al., 1999).

RT-PCR analysis

Total RNA was extracted from fly heads and their cDNA was synthesized with a SuperScript® III (Life Technologies). PCR amplification of dVPS35 was performed with 1 μl of cDNA solution and PrimeSTAR Max® DNA polymerase (Takara, Tokyo, Japan) with the following primer pairs: dVps35#2-F (5′-ATGGTTTGGATGACCAGGAGAAG-3′) in exon 1 and dVps35#2-R (5′-TCGTTCTCCTCAACCATCACATC-3′) in exon 3. Human αSYN was amplified using the set of primer pairs Syn-F (5′-TCGTGAGCGGAGAACTGGGAG-3′) and Syn-R (5′-TCAAGAAACTGGGAGCAAAGAT-3′) (Hasegawa et al., 2004). To normalize sample variations, the cDNA of ribosomal protein 49 (*rp49*), a housekeeping gene, was amplified using the primer pairs rp49-F (5′-AGCGCACCAAGCACTTCATCCGCCA-3′) and rp49-R (5′-GCGCACGTTGTGCACCAGGAACTTC-3′). After amplification, 10-ml aliquots were electrophoresed on 2.5% agarose gels, followed by photographic recording of the gels stained with ethidium bromide.

Immunohistochemistry

Sections of adult fly brain were immunostained according to the methods described previously (Feany and Bender, 2000). Briefly, 4-week-old adult flies were fixed in formalin and embedded in paraffin. To assess brain morphology, 5-μm frontal paraffin sections of heads were obtained and stained with hematoxylin and eosin. To evaluate the expression of human αSYN in the fly brain, anti-syn-1 monoclonal Ab (BD Bioscience) was applied at a 1:1000 dilution. Positive signals were detected by the avidin–biotin–peroxidase complex (Vectastain Elite ABC Kit, Vector Laboratories) method as described previously. The pictures were taken with a Biozero BZ-8000 digital microscope (Keyence, Tokyo, Japan). The numbers of αSYN-positive inclusions were counted per 15 × 15 μm^2 area in a defined area of the cortex (Kenyon cells) (Chen and Feany, 2005). Eight hemibrains were examined per genotype. The pooled data were statistically evaluated by a one-way ANOVA followed by a Bonferroni multiple comparison test.

Eye images

The eye phenotypes of 4-week-old anesthetized flies were evaluated. A minimum of 25 flies were evaluated for each genotype and conditions. Scanning electron microscopic images were obtained using a Miniscope TM-1000 (Hitachi, Tokyo, Japan). For the quantification of intact bristle numbers, a high-resolution image of a compound eye was printed, and the maximal visible surface was delimited (usually 300–500 ommatidia). The number of visible interommatidial bristles was counted and divided by the total number of ommatidia (Hilgers et al.,

2010). At least 10 eyes were analyzed for each genotype. The pooled data were statistically analyzed by a one-way ANOVA followed by a Bonferroni multiple comparison test.

Climbing assay

The climbing assay was performed, with slight modifications, according to published protocols (Feany and Bender, 2000). Ten to 20 male flies were placed into a conical glass tube (length, 15 cm; diameter, 2.5 cm) without anesthesia. Ten seconds after being tapped to the bottom of the tube, the number of flies in each vertical area was counted and scored as follows: score of 0 (0–2 cm), 1 (2–3.9 cm), 2 (4–5.9 cm), 3 (6–7.9 cm), 4 (8–9.9 cm), or 5 (10–15 cm). Five trials were performed in each group at 20 s intervals and the climbing index was calculated as follows: each score multiplied by the number of flies was divided by the total number of flies, and the mean score of each trial was calculated. The results are presented as the means ± standard errors of the scores obtained in 5–7 independent experiments. All climbing assay experiments were conducted at 25 °C. Pooled data from at least five independent experiments were statistically analyzed using a two-way ANOVA with a Bonferroni multiple comparison test.

Results

VPS35 RNAi alters CI-MPR distribution and impairs maturation of CTSD

The RNAi-mediated silencing of retromer subunits, such as VPS26 and Rab7, prevents the retrieval of unoccupied CI-MPR from endosomes to the TGN, leading to the lysosomal turnover of CI-MPR and a decrease in the cellular level of lysosomal hydrolases (Rojas et al., 2008). To determine whether the depletion of VPS35 also affects the intracellular distribution of CI-MPR, we downregulated VPS35 in HEK293 cells using two different siRNAs (#1 and #2) targeting *VPS35*. Consistent with previous findings (Rojas et al., 2008), the punctate signals of CI-MPR in cells expressing a normal level of endogenous VPS35 were preferentially localized in the perinuclear space, in which the TGN and late endosomes are usually located (Fig. 1A, left inset). In contrast, the CI-MPR signals in the VPS35-deficient cells were strikingly decreased and showed a more dispersed distribution in the periphery (Fig. 1A, right inset). As shown in Fig. 1B, human CTSD is first synthesized as pre-pro-CTSD, which is further converted to pro-CTSD (52 kDa), by the removal of the signal peptide, in the endoplasmic reticulum. The transport of pro-CTSD from the Golgi to the downstream acidic compartments is mainly mediated by the M6P pathway, i.e., the M6P residues on pro-CTSD are recognized by CI-MPR in the TGN, which segregates CTSD into transport vesicles that are delivered to the late endosomes and lysosomes. In late endosomes, pro-CTSD is processed to an intermediate form (48 kDa) and subsequently converted to mature CTSD (34 kDa) in lysosomes (Laurent-Matha et al., 2006). We confirmed that the ablation of the VPS35 component of the retromer by RNAi in HEK293 cells caused a considerable increase in intracellular pro-CTSD (indicated by an *asterisk*), whereas the amount of intracellular mature CTSD (indicated by an arrowhead) was markedly decreased. Notably, these changes were accompanied by a concomitant increase in pro-CTSD in the culture medium (Fig. 1C and D). The reduction in CI-MPR expression observed in VPS35-deficient cells implies a rerouting of CI-MPR to the lysosome for degradation, which is indicative of retromer dysfunction. As suggested by previous studies, the level of VPS26, a known interaction partner of VPS35, was substantially decreased in VPS35-silenced cells. The aberrant processing of CTSD in VPS35-deficient cells was further confirmed by an enzymatic assay showing that the activity of CTSD in VPS35 siRNA-treated cells was significantly lower than that in scrambled siRNA-treated cells (Fig. 1E).

VPS35 downregulation induces the αSYN accumulation in parallel with the reduction of mature CTSD in late endosomes and lysosomes

To examine whether CTSD effectively degrades αSYN in cultured cells, we over-expressed human CTSD in HEK293 cells that constitutively expressed human αSYN. When CTSD was highly overexpressed (3 μg of plasmid DNA per transfection) for 48 h, the level of mature CTSD was increased and the signal intensity of the monomeric, full-length αSYN (17 kDa) was significantly decreased (Fig. 2A, upper panel). Notably, in the presence of the protein synthesis inhibitor cycloheximide, the effect of CTSD on αSYN degradation was augmented and the amount of αSYN was significantly decreased in proportion to the dosage of CTSD expression (Fig. 2A, lower panel). Because pro-CTSD has a relatively long half-life (3–6 h) compared to αSYN (1.84 ± 0.16 h) (Bennett et al., 1999; Capony et al., 1989), it is likely that the cycloheximide blockage of protein synthesis did not affect CTSD levels dramatically. In agreement with a previous report (Cullen et al., 2009), the decrement in the αSYN monomer level was not accompanied by the appearance of low-molecular-weight αSYN fragments even with a long exposure of the immunoblot to the synuclein-1 Ab, which had previously shown reactivity with C-terminally truncated αSYN fragments *in vivo*. We used an MTT (3-(4,5-dimethylthiazo-2-yl)-2,5-diphenyltetrazolium bromide) assay to confirm that the observed effect of CTSD on lowering αSYN expression was not caused by impaired viability of the transfected cells (data not shown). In the second set of experiments, we examined whether the reduction in mature CTSD in response to *VPS35* knockdown altered the expression level of αSYN in the HEK293 cells stably expressing HA-tagged αSYN. Remarkably, the loss of VPS35 induced the accumulation of cellular HA-αSYN concomitant with incorrect processing of CTSD (Fig. 2B). The relative decrease in MPR in VPS35-depleted cells was interpreted as compromised retromer recruitment. Because CTSD is only active in an acidic environment, such as in late endosomes and lysosomes, serial fractionation was conducted to clarify the subcellular distribution of HA-αSYN in the *VPS35*-silenced cells. Thirty-six hours after silencing, the cells were harvested and sequentially fractionated into cytosol, endosome, and lysosome fractions. All samples were subjected to an immunoblot analysis, and the relative purity of the fractions was assessed using Abs directed against specific markers including Heat shock protein 90 (HSP90; cytosol), Rab5 (early endosome), and lysosome-associated membrane protein-2 (LAMP-2; lysosome). The results, shown in Fig. 2C, revealed that after silencing *VPS35*, the expression level of CI-MPR was slightly decreased in the endosomes but simultaneously increased downstream, in the lysosomal compartment. It

Fig. 1. Silencing of VPS35 caused a reduction in CI-MPR distribution and impaired maturation of CTSD. (A) The punctate signals of CI-MPR (red) in HEK293 cells expressing a normal level of endogenous VPS35 (green) were preferentially localized in the perinuclear space (left inset). In contrast, the signal of CI-MPR in VPS35-deficient cells was strikingly decreased and had a more dispersed distribution throughout the cell (right inset). White dotted lines show the contour of the cells. Nuclei were counterstained with DRAQ7. Scale bar: 10 μm. (B) Schematic diagram of the maturation process of CTSD. Human CTSD is first synthesized as pre-pro-CTSD, which is converted to pro-CTSD (52 kDa) by the removal of the signal peptide in the endoplasmic reticulum. The transport of pro-CTSD from the Golgi to the downstream acidic compartments is mainly mediated by the CI-MPR. In late endosomes, pro-CTSD is processed to an intermediate form (48 kDa) and subsequently converted to mature CTSD (34 kDa) in lysosomes. (C) The aberrant processing of CTSD in VPS35-deficient cells. The silencing of VPS35 by two different siRNAs (#1 and #2) in HEK293 cells caused a striking increase in the intracellular pro-CTSD (asterisk), whereas the amount of intracellular mature CTSD (arrowhead) was markedly decreased. This finding was accompanied by a concomitant increase in pro-CTSD in the medium. The left inset is CTSD with a longer exposure time. The reduction in CI-MPR expression observed in VPS35-deficient cells is indicative of retromer dysfunction. Note that the level of VPS26, another component of the retromer, was substantially decreased in VPS35-silenced cells. α-Tubulin and BSA were used as the internal controls for the total cell lysate and the medium, respectively. Representative blots from five independent experiments are presented. (D) The ratio of the densitometric values of mature/pro-CTSD both in cells and the medium is presented. Data are expressed as the means ± standard errors. $^{\dagger}p < 0.05$ and $^{\ddagger}p < 0.01$ (one-way ANOVA followed by Dunnett's test; $n = 5$). (E) The activity of CTSD in VPS35-specific siRNA (#1 and #2)-treated cells significantly declined compared to the activity in scrambled siRNA-treated cells. Data are expressed as the means ± standard errors. $^{\#}p < 0.05$ (one-way ANOVA followed by Dunnett's test; $n = 5$).

should be noted that the late endosome and lysosome share many features and both endosomal and lysosomal fractions are usually positive for LAMP2. The endosomal fraction isolated by our method contains both early and late endosomes because this fraction was positive for Rab5 and LAMP-2. In this study, the Rab5-negative, LAMP-2 positive component was defined as the lysosomal fraction. These findings suggest that in VPS35-depleted cells, the retromer fails to retrieve CI-MPR from the endosomes, resulting in the accumulation of CI-MPR in the lysosomes. CTSD was detected in both the endosome and lysosome fractions in HEK293 cells. However, after *VPS35* was silenced, the level of mature CTSD was substantially decreased in the lysosomes, whereas the pro-CTSD was upregulated in the endosomes. It is also interesting to note

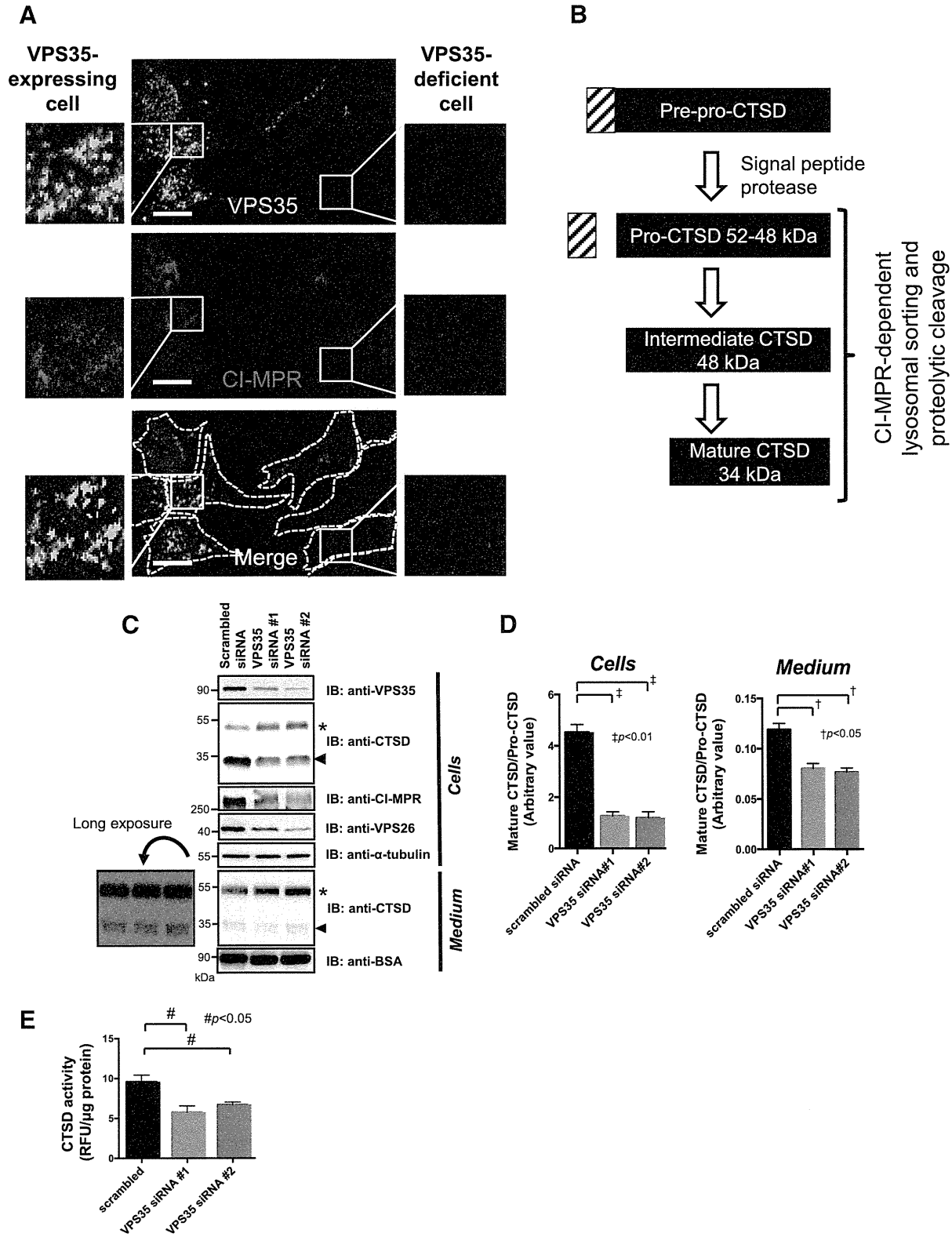

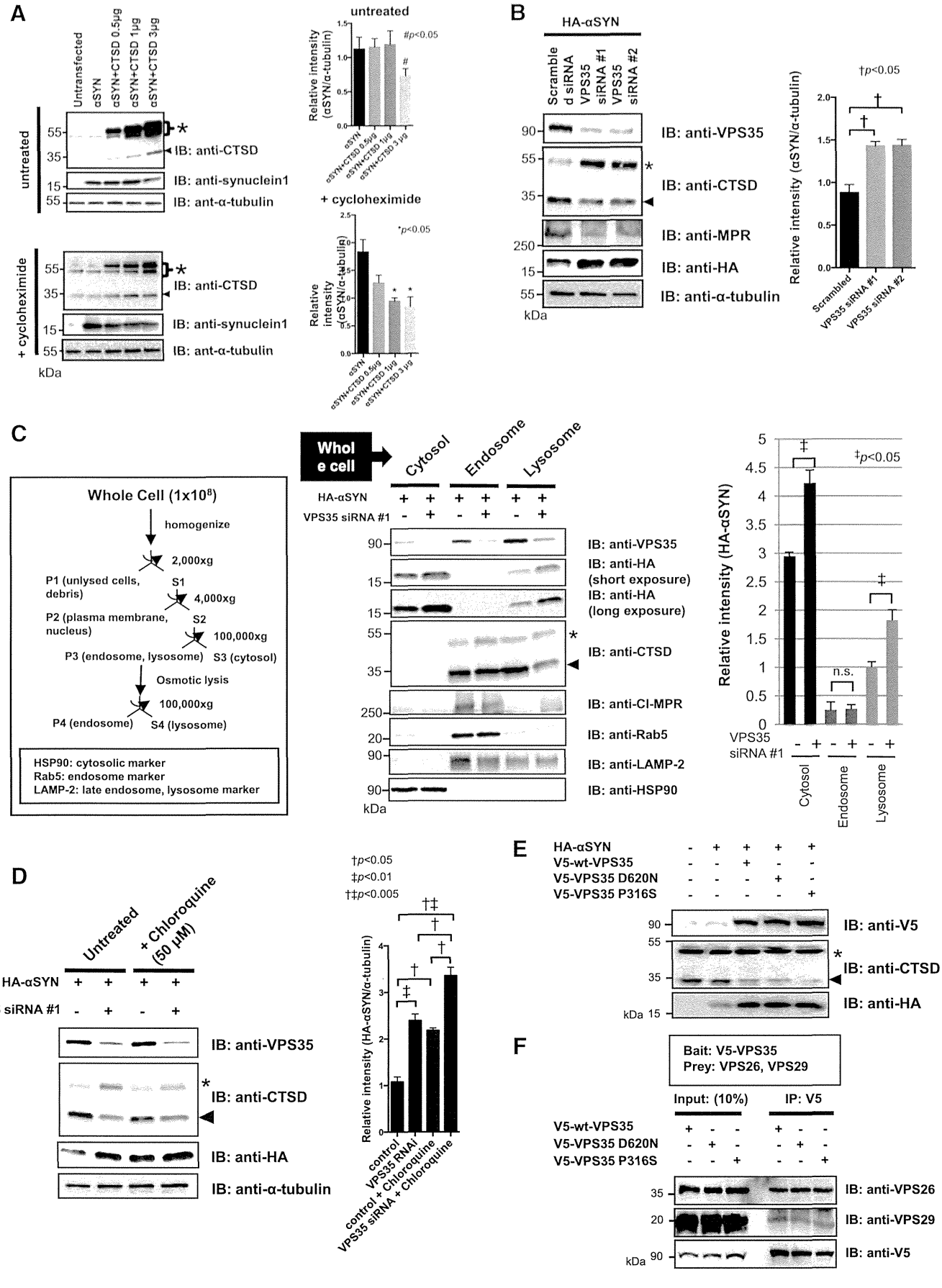
A
Untransfected
αSYN
αSYN+CTSD 0.5μg
αSYN+CTSD 1μg
αSYN+CTSD 3μg
untreated
+ cycloheximide
IB: anti-CTSD
IB: anti-synuclein1
IB: ant-α-tubulin
kDa
Relative intensity (αSYN/α-tubulin)
#p<0.05
*p<0.05
B
HA-αSYN
Scramble d siRNA
VPS35 siRNA #1
VPS35 siRNA #2
IB: anti-VPS35
IB: anti-CTSD
IB: anti-MPR
IB: anti-HA
IB: anti-α-tubulin
†p<0.05
Scrambled
VPS35 siRNA #1
VPS35 siRNA #2
C
Whole Cell (1x10⁸)
homogenize
2,000xg
P1 (unlysed cells, debris)
S1
4,000xg
P2 (plasma membrane, nucleus)
S2
100,000xg
P3 (endosome, lysosome)
S3 (cytosol)
Osmotic lysis
100,000xg
P4 (endosome)
S4 (lysosome)
HSP90: cytosolic marker
Rab5: endosome marker
LAMP-2: late endosome, lysosome marker
Whole cell
Cytosol
Endosome
Lysosome
VPS35 siRNA #1
IB: anti-VPS35
IB: anti-HA (short exposure)
IB: anti-HA (long exposure)
IB: anti-CTSD
IB: anti-CI-MPR
IB: anti-Rab5
IB: anti-LAMP-2
IB: anti-HSP90
Relative intensity (HA-αSYN)
n.s.
D
Untreated
+ Chloroquine (50 μM)
IB: anti-VPS35
IB: anti-CTSD
IB: anti-HA
IB: anti-α-tubulin
†p<0.05
‡p<0.01
††p<0.005
Relative intensity (HA-αSYN/α-tubulin)
control
VPS35 RNAi
control + Chloroquine
VPS35 siRNA + Chloroquine
E
V5-wt-VPS35
V5-VPS35 D620N
V5-VPS35 P316S
IB: anti-V5
IB: anti-CTSD
IB: anti-HA
F
Bait: V5-VPS35
Prey: VPS26, VPS29
Input: (10%)
IP: V5
IB: anti-VPS26
IB: anti-VPS29
IB: anti-V5

that treatment with chloroquine, a lysosomotropic agent that prevents endosomal acidification, further augmented the accumulation of HA-αSYN by VPS35 RNAi (Fig. 2D). This indicates that VPS35 knockdown does not completely inhibit lysosomal αSYN degradation. These observations indicate that if the retromer machinery is compromised, the pro-CTSD is entrapped in upstream structures and cannot be properly transported to the downstream acidic compartment. In an inverse correlation with the level of mature CTSD, the level of HA-αSYN was substantially upregulated in the lysosome fraction and the cytosol in the *VPS35*-silenced cells. Since autophagosomes should engulf cytosolic αSYN (Vogiatzi et al., 2008), increased cytosolic αSYN can be interpreted as the result of insufficient autophagic/lysosomal clearance of αSYN. To determine the possible effects of PD-linked mutations of *VPS35* on retromer function and αSYN degradation, we co-expressed HA-αSYN and mutant VPS35 (D620N and P316S) in HEK293 cells. Surprisingly, the over-expressed wt and the mutant VPS35 led to an equal αSYN accumulation, with no significant difference in the impaired maturation of CTSD (Fig. 2E). Furthermore, coimmunoprecipitation analyses of the wt and mutant VPS35 detected no differences in the binding affinity toward its known binding partners, VPS26 and VPS29 (Fig. 2F). Together, these findings indicate the essential role of the retromer machinery in lysosomal CTSD function in regulating the proteolytic pathway that is important for αSYN metabolism.

RNAi-mediated silencing of dVPS35 not only increased the insoluble αSYN species in brain but also deteriorated eye organization and locomotor function in human αSYN transgenic Drosophila

Although the retromer is implicated in PD pathogenesis, there is no evidence showing that deficiencies in the retromer sorting pathway cause the key phenotypes of the disease. Because the retromer complex is highly conserved and homologs have been found in yeast, nematode, fly, mouse, and human (Korolchuk et al., 2007), we investigated the effects of endogenous VPS35 on αSYN-induced neurotoxicity using flies that express the *h[wt]-SNCA* and *dVPS35* RNAi transgenes. The sequence-specific silencing of *dVPS35* in the fly brain was confirmed by RT-PCR (Fig. 3A). We found that the silencing of *dVPS35* strikingly increased the amount of the Triton-insoluble high-molecular-weight (HMW) αSYN species accompanied by a concomitant reduction in the level of Triton-soluble αSYN monomer in the brains of human αSYN-expressing flies under the panneural *embryonic lethal abnormal vision* (*elav*)-GAL4 driver (Fig. 3B). This finding is well corroborated by the immunohistochemical findings showing that the numbers of αSYN-positive inclusions in the fly cortex (Kenyon cells) were significantly increased in the brain of VPS35-deficient flies compared to controls (Fig. 3C). We attempted to detect human αSYN in the fly brain with or without proteinase K treatment, but did not observe a significant difference (data not shown). The mRNA levels in the brain of 4 fly lines were analyzed by RT-PCR (Fig. 3D). Note that the transcript levels of *h[wt]-SNCA* versus *rp49* were statistically identical between the *h[wt]-SNCA* × *GFP* RNAi and *h[wt]-SNCA* × *dVPS35* RNAi-1 fly lines. Furthermore, the cathepsin D activity in the brain was significantly decreased in *dVPS35* depleted flies (Fig. 3E). We then analyzed the eye phenotypes of flies expressing αSYN under the eye-specific *glass multiple reporter* (*GMR*)-GAL4 driver (Fig. 4A and B). When *dVPS35* was silenced, the human αSYN-Tg flies showed a slight shrinkage of each ommatidium with the loss of interommatidial bristles compared to control flies expressing both *h[wt]-SNCA* and *GFP* RNAi or both *EGFP* and *dVPS35* RNAi. We then investigated the impact of *dVPS35* silencing on the motor performance of flies that over-expressed human αSYN in the nervous system. For this purpose, we utilized a simple but powerful behavioral assay: the climbing assay. As shown in Fig. 5A and B, the flies overexpressing human wt-αSYN with *dVPS35* RNAi (*dVPS35* RNAi-1 and *dVPS35* RNAi-2) showed a significant, age-dependent deterioration in climbing ability compared to those expressing *GFP*-RNAi. Note that the flies that expressed αSYN in the absence of *dVPS35* did not have a shortened life span compared to the control flies (data not shown).

Discussion

In this study, we first showed that the silencing of *VPS35* in cultured cells caused a reduction in the distribution of CI-MPR and impaired the maturation of CTSD. Second, we found that the amount of pro-CTSD was substantially increased in the culture medium of the VPS35-deficient cells. Third, we demonstrated that silencing *VPS35* impairs the maturation of CTSD, which occurs concomitant with a striking accumulation of αSYN in lysosomes. Finally, we showed that the RNAi-mediated silencing of *dVPS35* not only induced the accumulation of the detergent-insoluble αSYN species in the brain but also exacerbated mild eye disorganization, as well as causing locomotor impairment in the flies expressing the human wild-type αSYN. Cumulatively, these data suggest that the retromer-dependent sorting machinery plays a role in αSYN catabolism by modulating the intracellular processing and activation of CTSD and might thereby contribute to the pathogenesis of PD (Fig. 6).

Although the evidence suggests that VPS35 is involved in the pathogenesis of PD, the mechanisms by which the mutant VPS35 causes retromer dysfunction and the subsequent neurodegeneration remain elusive. Given that the expression of VPS35 is significantly decreased in the brain regions selectively vulnerable to PD and AD and the studies in animal models (MacLeod et al., 2013; Muhammad et al., 2008; Small et al., 2005; Wen et al., 2011), the loss-of-function mechanism may explain the VPS35-related defective vesicle trafficking and subsequent neurodegeneration. As suggested by previous studies, our immunoprecipitation analyses indicate that the over-expressed VPS35 mutants (D620N and P316S) seem to maintain the binding capacity for the retromer subunits VPS26 and VPS29 (Vilarino-Guell et al., 2011). Nevertheless, the expression of the yeast VPS35 mutation (p.R98W) in the

Fig. 2. VPS35 depletion impairs the maturation of CTSD concomitantly with the accumulation of αSYN mainly in the late endosomes and lysosomes. (A) The level of exogenously expressed human αSYN (17 kDa) in HEK293 cells was decreased when the CTSD was highly over-expressed (3 μg plasmid for transfection) for 48 h (upper panel). Notably, under the existence of protein synthesis inhibitor cycloheximide, the effect of CTSD on αSYN degradation was augmented and the amount of αSYN was significantly decreased in proportion to the dosage of CTSD expression (lower panel). Pro-CTSD and mature CTSD are indicated by an asterisk and an arrowhead, respectively. Representative immunoblots from three independent experiments are shown. The densitometric quantification of αSYN versus α-tubulin is presented in the right panel. Data are expressed as the means ± standard errors. $^{\#,*}p < 0.05$ (one-way ANOVA followed by Dunnett's test; $n = 5$). (B) The depletion of VPS35 by siRNA (#1 and #2) induced the accumulation of intracellular HA-αSYN concomitant with the incorrect processing of CTSD in HEK293 cells stably expressing HA-αSYN. Pro-CTSD and mature CTSD are indicated by an asterisk and an arrowhead, respectively. Retromer dysfunction in VPS35-deficient cells was confirmed by the reduction in CI-MPR expression. Representative immunoblots from three independent experiments are presented. The relative band intensity of αSYN versus α-tubulin was calculated and is presented in the right panel. Data are expressed as the means ± standard errors. $^{\dagger}p < 0.05$ (one-way ANOVA followed by Dunnett's test; $n = 5$). (C) A marked increase in HA-αSYN in the lysosome fraction, as well as the cytosol, in *VPS35*-silenced HEK293 cells expressing HA-αSYN. Note that the expression level of CI-MPR was slightly decreased in the endosomes but simultaneously increased in the downstream lysosome compartments. CTSD was detected both in the endosome and lysosome fractions in HEK293 cells; however, after silencing *VPS35*, the level of mature CTSD (arrowhead) was substantially decreased in the lysosomes, whereas the pro-CTSD (asterisk) appeared upregulated in the endosomes. HSP90, Rab5, and LAMP-2 were used as the subcellular markers for the cytosol, endosome, and late endosome/lysosome, respectively. The fractionation and immunostaining were performed five times and exhibited consistent results. The densitometric quantification of HA-αSYN in each fraction is presented in the right panel. Data are expressed as the means ± standard errors. $^{\ddagger}p < 0.05$ (unpaired Student's *t*-test; $n = 5$). (D) Treatment with the lysosomal inhibitor, chloroquine (50 μM for 5 h), significantly augmented the accumulation of HA-αSYN by VPS35 RNAi. The relative band intensity of HA-αSYN versus α-tubulin is presented in the right panel. Data are expressed as the means ± standard errors. $^{\dagger}p < 0.05$ and $^{\ddagger}p < 0.01$ (one-way ANOVA followed by Dunnett's test; $n = 5$). (E) The over-expressed wt as well as mutant VPS35 in HEK293 cells equally led to αSYN accumulation, with no significant difference in the impaired CTSD maturation. (F) Coimmunoprecipitation analyses using HEK293 cells co-expressing wt and the mutant VPS35 detected no difference in the binding affinity toward its known binding partners, VPS26 and VPS29. Experiments were performed 3 times and yielded similar results.

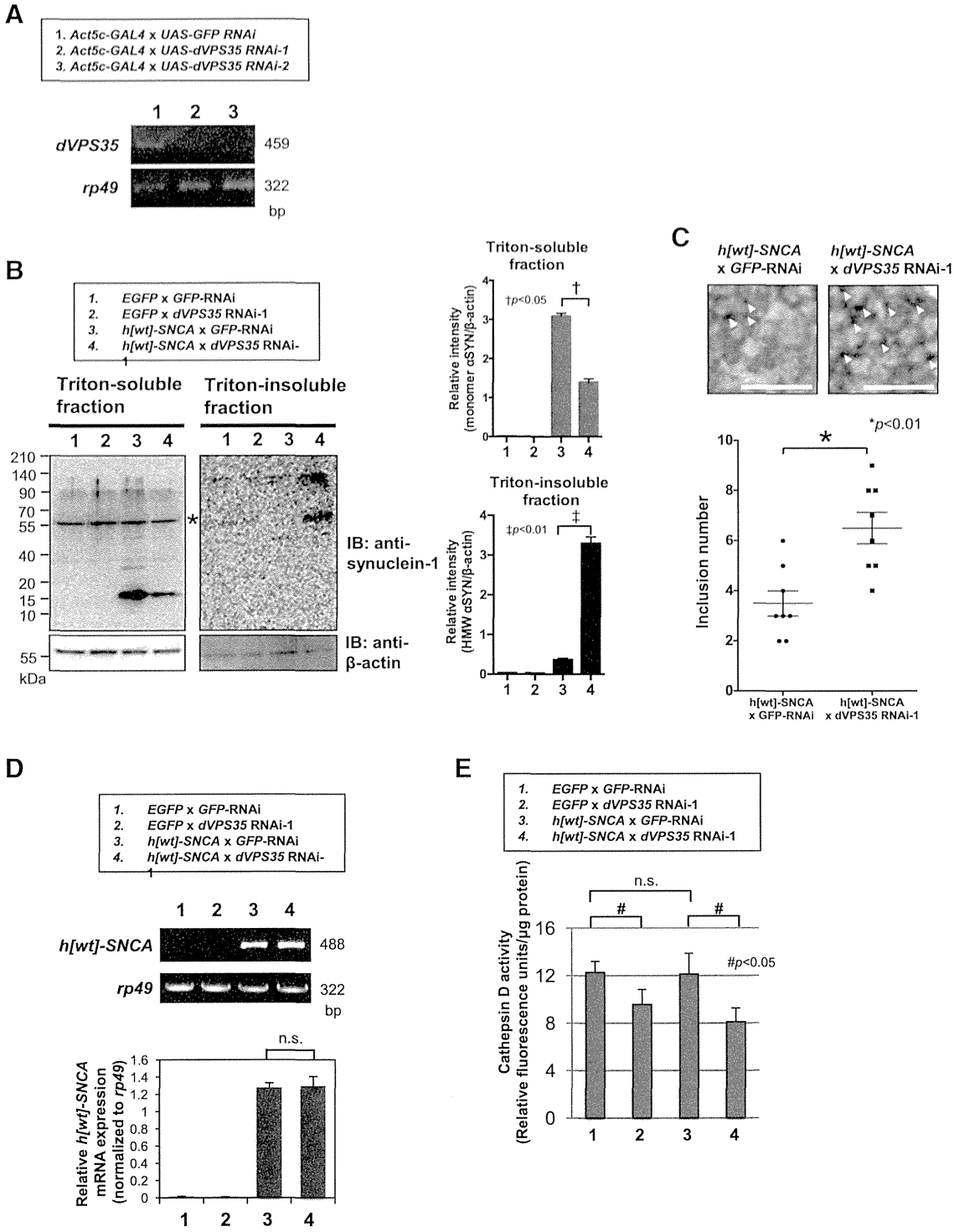

Fig. 3. Knockdown of *dVPS35* in human αSYN transgenic *Drosophila*. (A) Generation of *dVPS35*-knockdown flies. The sequence-specific silencing of *dVPS35* in the fly brain was confirmed by RT-PCR analysis. Ribosomal protein 49 (*rp49*), a housekeeping gene, was used as an internal control. RNAi-mediated knockdown was induced by *Act5c*-GAL4, which expresses GAL4 ubiquitously. (B) Neuron-specific knockdown of *dVPS35* affects the catabolism of the human wt αSYN. The *elav*-GAL4 driver was used for the transgene expression. Note that the silencing of *dVPS35* strikingly increased the amount of Triton-insoluble HMW αSYN species, which was accompanied by the concomitant reduction in Triton-soluble αSYN monomer in the brains of human αSYN-expressing flies under the *elav*-GAL4 driver. Equal loading was confirmed by an immunoblot using a β-actin Ab. An asterisk indicates the unspecific band that emerged due to the synuclein-1 Ab. The normalized band intensity data of monomeric αSYN in the Triton-soluble fraction (gray bar) as well as the HMW αSYN (above 100 kDa) in the Triton-insoluble fraction (black bar) are presented in the right panel. Data are expressed as the means ± standard errors. $^{\dagger}p < 0.05$ and $^{\ddagger}p < 0.01$ (one-way ANOVA followed by Dunnett's test; $n = 5$). (C) The immunohistochemical staining of fly brains using a human αSYN-specific antibody. The αSYN-positive inclusions (arrowhead) were counted in a defined area of the cortex (Kenyon cell). Note that the numbers of αSYN-positive inclusions in the fly cortex were significantly increased in the brain of VPS35-deficient flies compared to controls. Scale bar: 10 μm. (D) The mRNA levels in the brains of 4 fly lines were analyzed by RT-PCR. *Rp49* was used as an internal control. Note that the transcript levels of *h[wt]-SNCA* are statistically identical between the *h[wt]-SNCA* × *GFP* RNAi and *h[wt]-SNCA* × *dVPS35* RNAi-1 fly lines. The relative *h[wt]-SNCA* mRNA expression levels normalized to *rp49* were calculated. Data are expressed as the means ± standard errors (one-way ANOVA followed by Dunnett's test; $n = 5$). (E) The CTSD activity in the brain was significantly decreased in *dVPS35* depleted flies. Results are presented as means ± standard errors. $^{\#}p < 0.05$ (one-way ANOVA with the post-hoc Dunnett's test; $n = 5$).

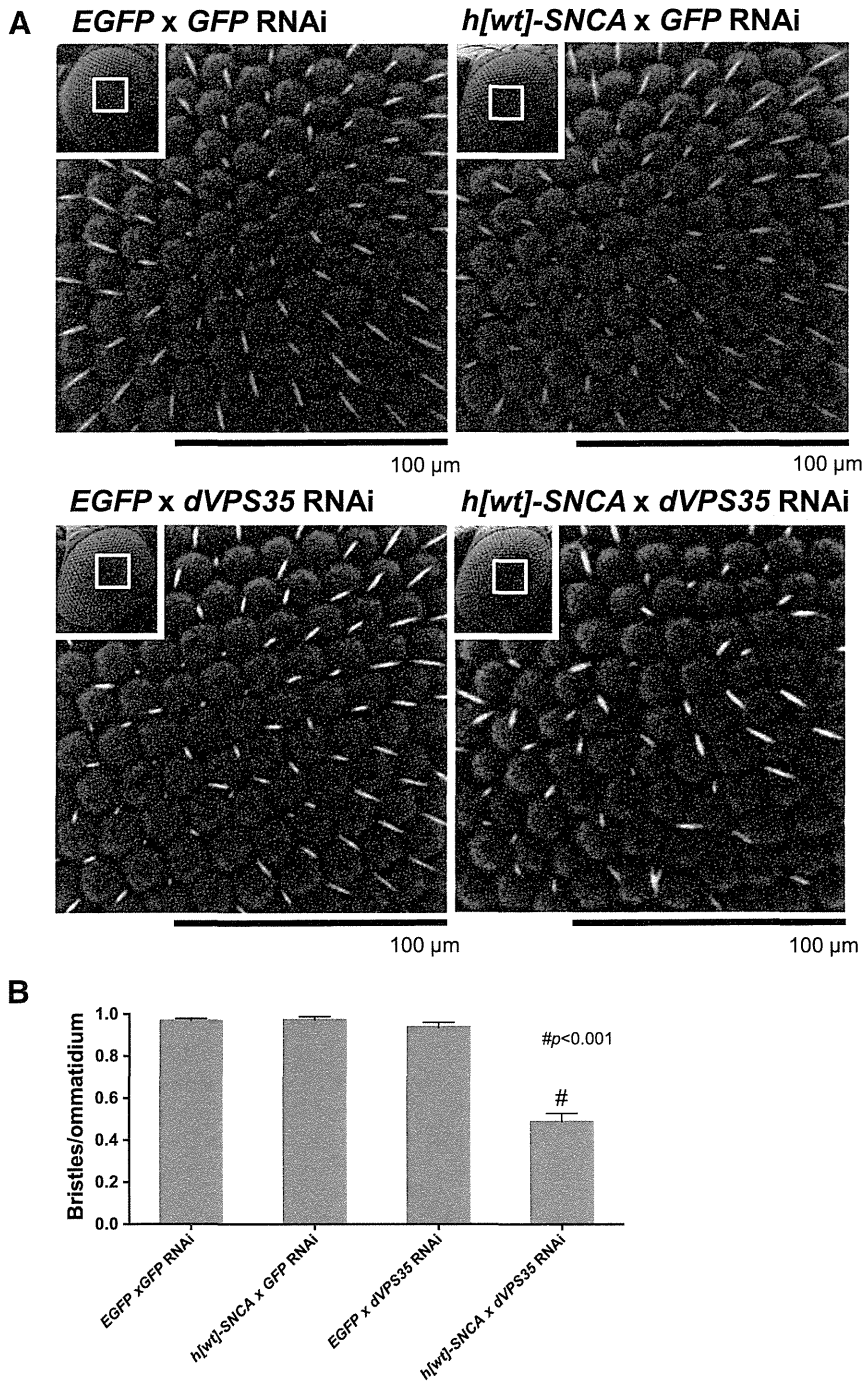

Fig. 4. Silencing of *dVPS35* induces mild eye disorganization in human αSYN transgenic *Drosophila*. (A) Eye-specific expression of *h[wt]-SNCA* with *dVPS35* RNAi resulted in compound eye disorganization. The eye phenotype was normal in 1-week-old transgenic flies over-expressing *h[wt]-SNCA* with *GFP* RNAi. By contrast, when *dVPS35* was silenced, the *h[wt]-SNCA*-Tg flies showed a slight shrinkage of each ommatidium with disarrayed bristles compared to the control flies expressing both *h[wt]-SNCA* and *GFP* RNAi or both *EGFP* and *dVPS35* RNAi. The white square indicates the magnified area. Scale bar: 100 μm. (B) For the quantification of intact interommatidial bristle numbers, the number of visible bristles was counted and divided by the total number of ommatidium. Note that the silencing of dVPS35 in SNCA transgenic flies significantly decreased the numbers of bristles compared to other fly lines. The pooled data were statistically analyzed by a one-way ANOVA followed by a Bonferroni multiple comparison test. $^{\#}p < 0.001$ ($n \geq 10$).

highly conserved PRLYL motif at the N-terminus destabilizes VPS26 and disrupts cargo sorting in the prevacuolar endosome and retrieval of the retromer to the TGN, indicating that this mutation converts VPS35 to a dominant-negative protein in *Saccharomyces cerevisiae* (Zhao et al., 2007). Similarly, in a rat insulinoma cell line, the exogenous expression of the human VPS35 R107W mutant (the functional equivalent of the R98 residue in yeast) has an altered intracellular membrane distribution that perturbs a number of post-Golgi trafficking functions (Zhao et al., 2007). Moreover, a recent study has shown that the expression of D620N VPS35 induces the marked degeneration of dopaminergic neurons both in primary neuron culture and in a rat model (Tsika et al., 2014). These findings suggest that mutant VPS35 may have an influence on retromer function via a potentially toxic gain-of-function with a dominant negative effect. This notion is supported by a recent observation demonstrating that the PD-linked *VPS35* D620N mutation disrupts the cargo-sorting function of the retromer, causing an abnormal trafficking of CTSD (Follett et al., 2014). We also produced the overexpression of the PD-linked mutant VPS35 (D620N and P316S) in

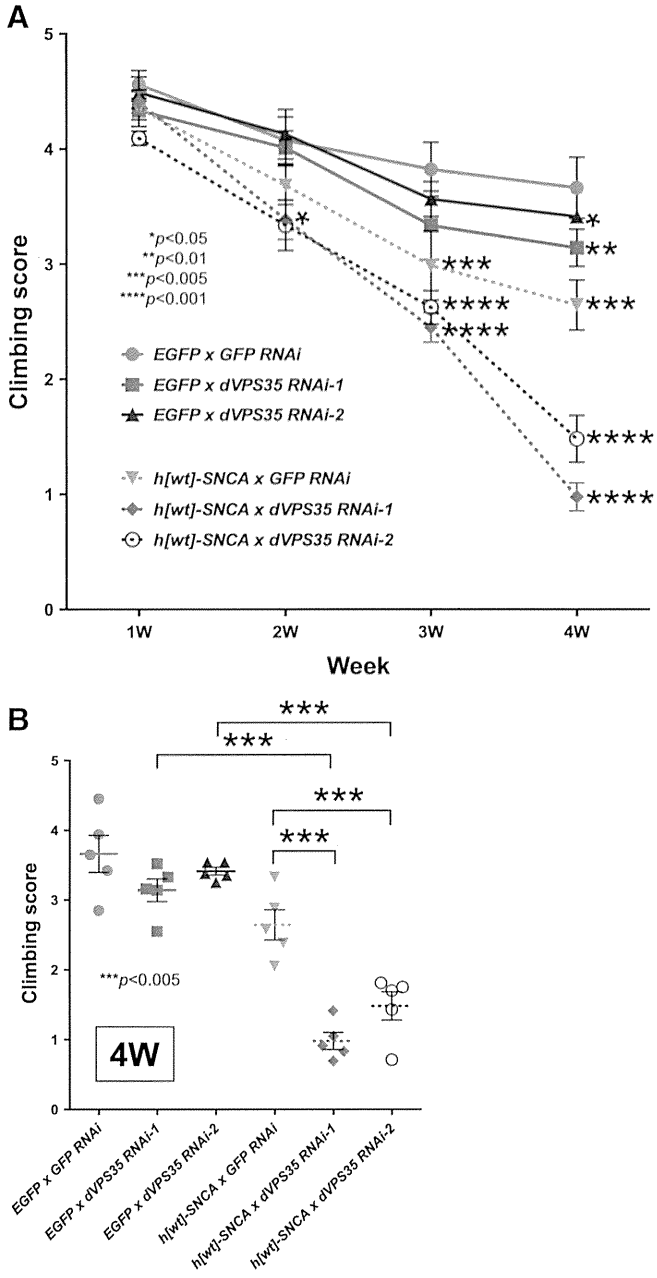

Fig. 5. RNAi-mediated silencing of *dVPS35* deteriorates locomotor function in human αSYN transgenic *Drosophila*. (A) Knockdown of *dVPS35* induced an age-dependent decline in climbing performance in flies expressing the human αSYN in the nervous system. Five trials were performed in each group at 20 s intervals and the climbing index was calculated. Results are presented as the means ± standard errors of the scores obtained in 5–10 independent experiments. All climbing assay experiments were conducted at 25 °C. The *Elav*-GAL4 driver was used for the experiment. (B) In order to make it easier to compare each climbing performance in different fly lines, the climbing scores of 4-week-old flies are also presented as a categorized scatter plot with mean segments. Pooled data from at least 5 experiments were statistically analyzed. $^{*}p < 0.05$, $^{**}p < 0.01$, $^{***}p < 0.005$, and $^{****}p < 0.001$ (two-way ANOVA with the Bonferroni multiple comparison test; $n \geq 5$).

HEK293 cells to determine its distinct influence on retromer function. Unexpectedly, not only the exogenously expressed mutants, but also the wt VPS35 equally resulted in the aberrant trafficking of CI-MPR together with the impaired maturation of CTSD. This finding is apparently contradictory to a report by Follett et al., which demonstrated that exogenous expression of the mutant D620N, but not the wt VPS35, abnormally traffics CI-MPR in HEK293 cells, resulting in the incorrect processing of CTSD. Although the reasons for these discrepancies are not clear, a possible explanation is the difference in the protein expression level in each experiment. The retromer requires an apparent equimolar stoichiometry of the subunit to exert its normal function (Hierro et al., 2007; Seaman et al., 2009). Thus, it is possible that even the wt VPS35 may be able to negatively perturb the function of the retromer when heavily over-expressed.

Regardless of the modes of gene action, the genetic modification of VPS35 can result in the disruption of retromer function and the aberrant trafficking of cargo proteins such as CI-MPR. CI-MPR appears to be the primary receptor for the major lysosomal 'α-synucleinase' CTSD that is abundantly expressed in the brain (Ludwig et al., 1994; Press et al., 1998). Indeed, Sevlever et al. found that the main degradation activity of αSYN in the lysosomal fractions from cultured neurons was greatly inhibited by the CTSD inhibitor pepstatin A (Sevlever et al., 2008). They showed that other protease inhibitors such as leupeptin weakly reduced αSYN degradation. This result indicates that in addition to CTSD, other proteolytic activities play a role in αSYN degradation within lysosomes. This notion is corroborated by our data showing that treatment of the lysosomal inhibitor chloroquine slightly but significantly augmented αSYN levels in cells transfected with VPS35 siRNA. Nevertheless, the altered processing and prominent accumulation of insoluble species of endogenous αSYN in three different mammals with CTSD deficiency indicate that its enzyme activity plays a fundamental role in αSYN metabolism (Cullen et al., 2009). Although both the proteasome and the lysosome have been proposed to play a role in the degradation of αSYN (Ebrahimi-Fakhari et al., 2011; Konno et al., 2012), recent observations have underscored the contribution of the autophagy–lysosome pathway (Mak et al., 2010; Vogiatzi et al., 2008). CTSD, lysosome-associated membrane protein-1 (LAMP-1), and heat shock protein 73 (Hsp73) immunoreactivities are significantly decreased (approximately 50% versus control) in the substantia nigra neurons of idiopathic PD patients (Chu et al., 2009). Furthermore, parkinsonism has been noted in lysosomal deficiencies such as the adult forms of neuronal ceroid lipofuscinosis, Gaucher disease, and Kufor–Rakeb syndrome (Schneider and Zhang, 2010). The CTSD deficiency is thought to broadly influence the lysosomal and autophagic degradation of its substrate proteins (Koike et al., 2000). Moreover, recent work has revealed that the D620N mutant VPS35 fails to associate with the WASH (Wiskott–Aldrich syndrome protein and SCAR homolog) complex, an important regulator of vesicle trafficking. This failure impairs the autophagic clearance of huntingtin proteins with Q74 repeats and the A53T mutant of αSYN (Zavodszky et al., 2014), raising the question of how the impaired autophagic–lysosomal degradation by retromer dysfunction can specifically lead to αSYN accumulation. One possible mechanism is the involvement of the chaperone-mediated autophagy (CMA). Indeed, the amino acid sequence of αSYN contains a pentapeptide succession consistent with a CMA recognition motif and *in vitro* experiments demonstrated that this motif is essential for the internalization of αSYN into the lysosomal lumen and for degradation by lysosomal proteases (Cuervo et al., 2004). Another regulatory mechanism which may control the selective sorting and degradation of αSYN in lysosomes is the ubiquitin-modification. It has been shown that Nedd4 (neural precursor cell expressed developmentally down-regulated protein 4), a ubiquitin E3 ligase that targets protein substrates to lysosomes, catalyzes K63-mediated αSYN ubiquitination and enhances its clearance in lysosomes (Sugeno et al., 2014; Tofaris et al., 2011). Moreover, the over-expression of wt-Nedd4 reduces αSYN accumulation in the nervous tissue and induces neurodegeneration and locomotor abnormality in both fly and rat models (Davies et al., 2014). This finding is well corroborated by the yeast model experiment showing that N-aryl benzimidazole (NAB) strongly and selectively counteracts the αSYN cytotoxicity through its influence on Rsp5, a yeast homolog of Nedd4 (Tardiff et al., 2013). Our experiments using a novel fly model of VPS35-linked PD provide evidence for a modulatory effect of endogenous VPS35 expression on αSYN toxicity *in vivo*. Despite the lack of direct evidence showing that fruit fly CTSD accepts human αSYN as a substrate, we found that the knockdown of dVPS35 significantly

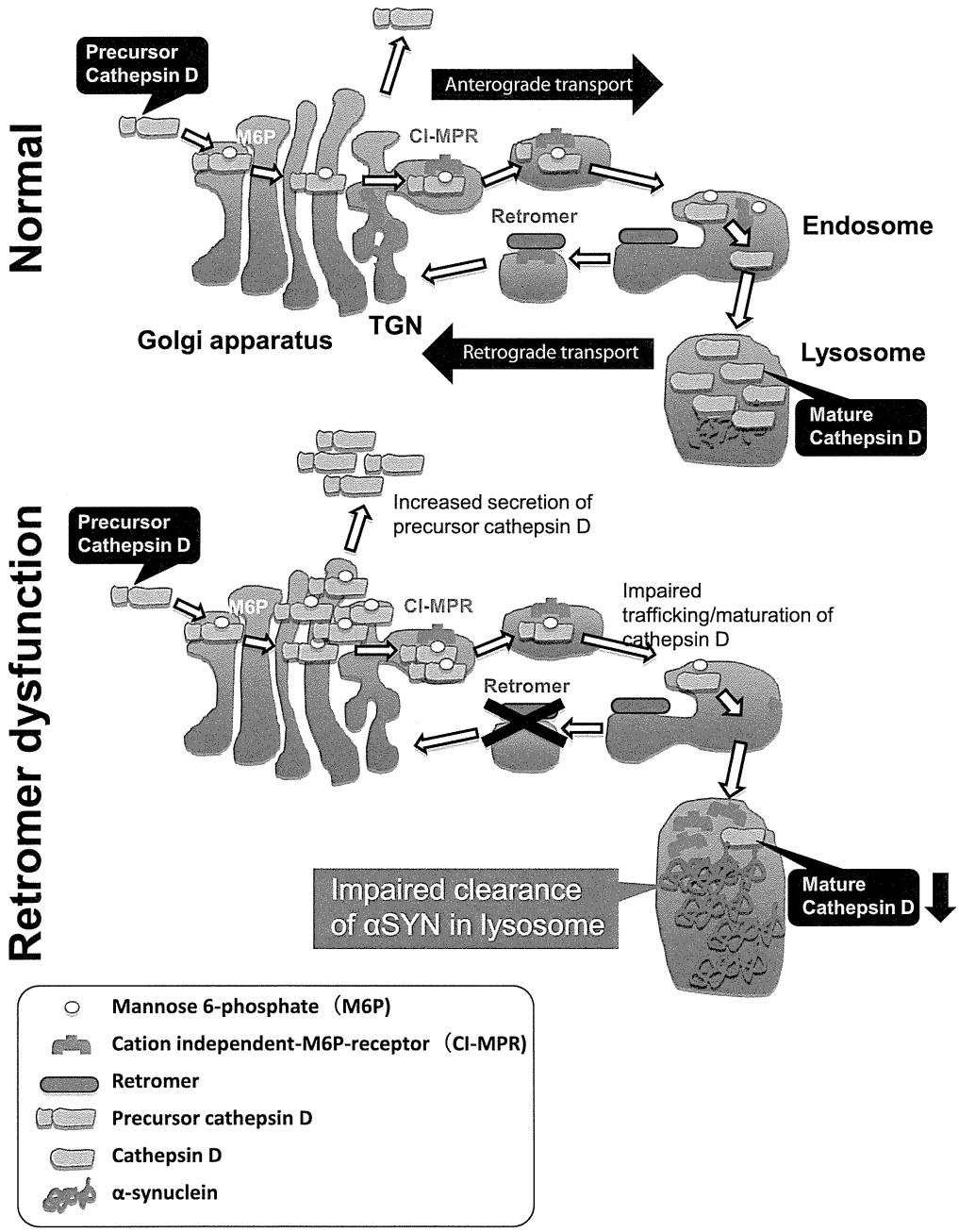

Fig. 6. Schematic illustrations of retromer-mediated trafficking of CTSD and possible contribution to lysosomal αSYN degradation. VPS35, a critical component of the retromer complex, mediates retrograde transport of cargo protein (CI-MPR) from endosome to the TGN. Under physiological condition (upper panel), upon arrival in the Golgi apparatus, newly synthesized CTSD precursor is specifically modified with M6P residues, which are recognized by CI-MPR in the TGN. CI-MPR escorts CTSD into endosomes, in which the CTSD are released for further transport to lysosomes. During this process, CTSD is activated by the proteolytic cleavage of the signal peptide sequence. The retromer retrieves the unoccupied MPRs from endosomes to the TGN, where they participate in further cycles of CTSD sorting. If the retromer function is perturbed (lower panel), the retromer fails to retrieve CI-MPR from the endosome to the TGN, which results in increased secretion of precursor CTSD as well as the impaired trafficking of CTSD. As a consequence, the amount of mature CTSD in the lysosome is decreased, which increases the accumulation of αSYN and might influence the neurodegenerative process linked to PD.

lowered the CTSD activity in fly brain and the deletion of the homologous CTSD-encoding gene in the fly promoted the toxicity of the ectopically expressed human αSYN in the fly retina (Cullen et al., 2009). These observations suggest that the altered expression level of dVPS35 may interfere with CTSD activation and thereby have an effect on the cellular burden of αSYN. Indeed, the accumulation of the HMW Triton-insoluble αSYN species accompanied by a decrease in soluble monomeric αSYN in our fly model is consistent with the results in CTSD-deficient mouse brain showing that the level of soluble endogenous αSYN was reduced, whereas the levels of insoluble, oligomeric αSYN species were increased (Cullen et al., 2009). The reason that the αSYN monomer was decreased in the dVPS35-deficient fly brain whereas the monomeric αSYN was increased in VPS35-silenced HEK293 cells is uncertain. However, it is possible that the long-lasting CTSD deficiency caused by retromer malfunction may facilitate the buildup of the HMW αSYN species. The eye phenotype of the dVPS35-deficient αSYN transgenic fly is relatively mild compared to that of CTSD-knockout flies that showed age-dependent vacuolar degeneration and thinning of the retinal architecture (Cullen et al., 2009). Furthermore, the life span of our flies was roughly comparable to that of normal flies, whereas the CTSD-knockdown flies manifested a clearly shortened life span (Tsakiri et al., 2013). Presumably, there may be an inverse

correlation between the severity of the disease and the level of residual CTSD enzyme activity. The observed mild eye degeneration and the age-dependent decline of motor performance in αSYN Tg flies with a dVPS35-null background may recapitulate the slowly progressive feature of the human disease. Although the underlying molecular mechanism by which VPS35 deficiency facilitates eye disorganization and progressive motor disability in human αSYN Tg flies remains enigmatic, there is substantial evidence to suggest that the toxic conversion of αSYN from soluble monomers to aggregated, insoluble forms in the brain is a key event in the pathogenesis of PD and related diseases (Cookson, 2005). Thus, the intracellular buildup of the potentially noxious αSYN species in the fly brain may partly provide a plausible explanation for the cytotoxicity.

In summary, we found that retromer depletion impaired CTSD maturation in parallel with the accumulation of αSYN in lysosomes. Moreover, the newly established fly model of *VPS35*-linked PD provided evidence for a possible modulatory effect of endogenous VPS35 expression on αSYN toxicity *in vivo*. Interestingly, MacLeod et al. (2013) have demonstrated that wt VPS35 (PARK17) could rescue the phenotypes caused by LRRK2 (PARK8) or RAB7L1 (PARK16) risk variants both *in vitro* and *in vivo*. Furthermore, the locomotor abnormalities and shortened lifespan in flies expressing mutant human LRRK2 can be rescued by the overexpression of VPS35 (Linhart et al., 2014). These findings indicate that these PD-associated genes may configure a common cellular pathway. The functional interrelationship of the endo-lysosomal system in PD is also highlighted by the recent identification of pathogenic mutations in *DNAJC6* and *DNAJC13*, recently identified genes encoding the DNAJ domain-bearing proteins involved in endosomal trafficking, in rare familial forms of PD (Edvardson et al., 2012; Vilarino-Guell et al., 2014). Further studies will be required to gain insight into the pathophysiological role of the endocytosis and endo/lysosomal trafficking systems in synucleinopathy and to identify molecular targets for potential therapeutic interventions.

Acknowledgments

The authors thank Dr. Matthew J. Farrer (Centre of Applied Neurogenetics, University of British Columbia, Canada) for providing the human wt and mutant (D620N and P316S) VPS35 constructs. This work was supported in part by a Grant-in-Aid for Scientific Research (C) [grant number 26461263], a Grant-in-Aid for Scientific Research (B) [grant number 24390219], and a Grant-in-Aid for Exploratory Research [grant number 24659423] from the Ministry of Education, Culture, Sports, Science and Technology (MEXT); a grant from the Research Committee for Ataxic Diseases, a Grant-in-Aid for Scientific Research on Innovative Areas (Brain Environment) [grant number 24111502] from the Ministry of Health, Labor, and Welfare, Japan; and the Intramural Research Grant [grant number 24-5] for Neurological and Psychiatric Disorders of the National Center of Neurology and Psychiatry (NCNP), Japan.

References

Bennett, M.C., Bishop, J.F., Leng, Y., Chock, P.B., Chase, T.N., Mouradian, M.M., 1999. Degradation of alpha-synuclein by proteasome. J. Biol. Chem. 274, 33855–33858.

Capony, F., Rougeot, C., Montcourrier, P., Cavailles, V., Salazar, G., Rochefort, H., 1989. Increased secretion, altered processing, and glycosylation of pro-cathepsin D in human mammary cancer cells. Cancer Res. 49, 3904–3909.

Chen, L., Feany, M.B., 2005. Alpha-synuclein phosphorylation controls neurotoxicity and inclusion formation in a Drosophila model of Parkinson disease. Nat. Neurosci. 8, 657–663.

Chu, Y., Dodiya, H., Aebischer, P., Olanow, C.W., Kordower, J.H., 2009. Alterations in lysosomal and proteasomal markers in Parkinson's disease: relationship to alpha-synuclein inclusions. Neurobiol. Dis. 35, 385–398.

Cookson, M.R., 2005. The biochemistry of Parkinson's disease. Annu. Rev. Biochem. 74, 29–52.

Cuervo, A.M., Stefanis, L., Fredenburg, R., Lansbury, P.T., Sulzer, D., 2004. Impaired degradation of mutant alpha-synuclein by chaperone-mediated autophagy. Science 305, 1292–1295.

Cullen, V., Lindfors, M., Ng, J., Paetau, A., Swinton, E., Kolodziej, P., Boston, H., Saftig, P., Woulfe, J., Feany, M.B., Myllykangas, L., Schlossmacher, M.G., Tyynela, J., 2009. Cathepsin D expression level affects alpha-synuclein processing, aggregation, and toxicity in vivo. Mol. Brain 2, 5.

Davies, S.E., Hallett, P.J., Moens, T., Smith, G., Mangano, E., Kim, H.T., Goldberg, A.L., Liu, J.L., Isacson, O., Tofaris, G.K., 2014. Enhanced ubiquitin-dependent degradation by Nedd4 protects against alpha-synuclein accumulation and toxicity in animal models of Parkinson's disease. Neurobiol. Dis. 64, 79–87.

Dehay, B., Martinez-Vicente, M., Caldwell, G.A., Caldwell, K.A., Yue, Z., Cookson, M.R., Klein, C., Vila, M., Bezard, E., 2013. Lysosomal impairment in Parkinson's disease. Mov. Disord. 28, 725–732.

Ebrahimi-Fakhari, D., Cantuti-Castelvetri, I., Fan, Z., Rockenstein, E., Masliah, E., Hyman, B.T., McLean, P.J., Unni, V.K., 2011. Distinct roles in vivo for the ubiquitin–proteasome system and the autophagy-lysosomal pathway in the degradation of alpha-synuclein. J. Neurosci. 31, 14508–14520.

Edvardson, S., Cinnamon, Y., Ta-Shma, A., Shaag, A., Yim, Y.I., Zenvirt, S., Jalas, C., Lesage, S., Brice, A., Taraboulos, A., Kaestner, K.H., Greene, L.E., Elpeleg, O., 2012. A deleterious mutation in DNAJC6 encoding the neuronal-specific clathrin-uncoating co-chaperone auxilin, is associated with juvenile parkinsonism. PLoS One 7, e36458.

Feany, M.B., Bender, W.W., 2000. A Drosophila model of Parkinson's disease. Nature 404, 394–398.

Follett, J., Norwood, S.J., Hamilton, N.A., Mohan, M., Kovtun, O., Tay, S., Zhe, Y., Wood, S.A., Mellick, G.D., Silburn, P.A., Collins, B.M., Bugarcic, A., Teasdale, R.D., 2014. The Vps35 D620N mutation linked to Parkinson's disease disrupts the cargo sorting function of retromer. Traffic 15, 230–244.

Hasegawa, T., Matsuzaki, M., Takeda, A., Kikuchi, A., Akita, H., Perry, G., Smith, M.A., Itoyama, Y., 2004. Accelerated alpha-synuclein aggregation after differentiation of SH-SY5Y neuroblastoma cells. Brain Res. 1013, 51–59.

Hasegawa, T., Matsuzaki-Kobayashi, M., Takeda, A., Sugeno, N., Kikuchi, A., Furukawa, K., Perry, G., Smith, M.A., Itoyama, Y., 2006. Alpha-synuclein facilitates the toxicity of oxidized catechol metabolites: implications for selective neurodegeneration in Parkinson's disease. FEBS Lett. 580, 2147–2152.

Hasegawa, T., Baba, T., Kobayashi, M., Konno, M., Sugeno, N., Kikuchi, A., Itoyama, Y., Takeda, A., 2010. Role of TPPP/p25 on alpha-synuclein-mediated oligodendroglial degeneration and the protective effect of SIRT2 inhibition in a cellular model of multiple system atrophy. Neurochem. Int. 57, 857–866.

Hasegawa, T., Konno, M., Baba, T., Sugeno, N., Kikuchi, A., Kobayashi, M., Miura, E., Tanaka, N., Tamai, K., Furukawa, K., Arai, H., Mori, F., Wakabayashi, K., Aoki, M., Itoyama, Y., Takeda, A., 2011. The AAA-ATPase VPS4 regulates extracellular secretion and lysosomal targeting of alpha-synuclein. PLoS One 6, e29460.

Hierro, A., Rojas, A.L., Rojas, R., Murthy, N., Effantin, G., Kajava, A.V., Steven, A.C., Bonifacino, J. S., Hurley, J.H., 2007. Functional architecture of the retromer cargo-recognition complex. Nature 449, 1063–1067.

Hilgers, V., Bushati, N., Cohen, S.M., 2010. Drosophila microRNAs 263a/b confer robustness during development by protecting nascent sense organs from apoptosis. PLoS Biol. 8, e1000396.

Koike, M., Nakanishi, H., Saftig, P., Ezaki, J., Isahara, K., Ohsawa, Y., Schulz-Schaeffer, W., Watanabe, T., Waguri, S., Kametaka, S., Shibata, M., Yamamoto, K., Kominami, E., Peters, C., von Figura, K., Uchiyama, Y., 2000. Cathepsin D deficiency induces lysosomal storage with ceroid lipofuscin in mouse CNS neurons. J. Neurosci. 20, 6898–6906.

Konno, M., Hasegawa, T., Baba, T., Miura, E., Sugeno, N., Kikuchi, A., Fiesel, F.C., Sasaki, T., Aoki, M., Itoyama, Y., Takeda, A., 2012. Suppression of dynamin GTPase decreases alpha-synuclein uptake by neuronal and oligodendroglial cells: a potent therapeutic target for synucleinopathy. Mol. Neurodegener. 7, 38.

Korolchuk, V.I., Schutz, M.M., Gomez-Llorente, C., Rocha, J., Lansu, N.R., Collins, S.M., Wairkar, Y.P., Robinson, I.M., O'Kane, C.J., 2007. Drosophila Vps35 function is necessary for normal endocytic trafficking and actin cytoskeleton organisation. J. Cell Sci. 120, 4367–4376.

Laurent-Matha, V., Derocq, D., Prebois, C., Katunuma, N., Liaudet-Coopman, E., 2006. Processing of human cathepsin D is independent of its catalytic function and autoactivation: involvement of cathepsins L and B. J. Biochem. 139, 363–371.

Lee, B.R., Kamitani, T., 2011. Improved immunodetection of endogenous alpha-synuclein. PLoS One 6, e23939.

Linhart, R., Wong, S.A., Cao, J., Tran, M., Huynh, A., Ardrey, C., Park, J.M., Hsu, C., Taha, S., Peterson, R., Shea, S., Kurian, J., Venderova, K., 2014. Vacuolar protein sorting 35 (Vps35) rescues locomotor deficits and shortened lifespan in Drosophila expressing a Parkinson's disease mutant of Leucine-rich repeat kinase 2 (LRRK2). Mol. Neurodegener. 9, 23.

Ludwig, T., Munier-Lehmann, H., Bauer, U., Hollinshead, M., Ovitt, C., Lobel, P., Hoflack, B., 1994. Differential sorting of lysosomal enzymes in mannose 6-phosphate receptor-deficient fibroblasts. EMBO J. 13, 3430–3437.

MacLeod, D.A., Rhinn, H., Kuwahara, T., Zolin, A., Di Paolo, G., McCabe, B.D., Marder, K.S., Honig, L.S., Clark, L.N., Small, S.A., Abeliovich, A., 2013. RAB7L1 interacts with LRRK2 to modify intraneuronal protein sorting and Parkinson's disease risk. Neuron 77, 425–439.

Mak, S.K., McCormack, A.L., Manning-Bog, A.B., Cuervo, A.M., Di Monte, D.A., 2010. Lysosomal degradation of alpha-synuclein in vivo. J. Biol. Chem. 285, 13621–13629.

Muhammad, A., Flores, I., Zhang, H., Yu, R., Staniszewski, A., Planel, E., Herman, M., Ho, L., Kreber, R., Honig, L.S., Ganetzky, B., Duff, K., Arancio, O., Small, S.A., 2008. Retromer deficiency observed in Alzheimer's disease causes hippocampal dysfunction, neurodegeneration, and Abeta accumulation. Proc. Natl. Acad. Sci. U. S. A. 105, 7327–7332.

Poewe, W., Mahlknecht, P., 2009. The clinical progression of Parkinson's disease. Parkinsonism Relat. Disord. 15 (Suppl. 4), S28–S32.

Press, B., Feng, Y., Hoflack, B., Wandinger-Ness, A., 1998. Mutant Rab7 causes the accumulation of cathepsin D and cation-independent mannose 6-phosphate receptor in an early endocytic compartment. J. Cell Biol. 140, 1075–1089.

Rojas, R., van Vlijmen, T., Mardones, G.A., Prabhu, Y., Rojas, A.L., Mohammed, S., Heck, A.J., Raposo, G., van der Sluijs, P., Bonifacino, J.S., 2008. Regulation of retromer recruitment to endosomes by sequential action of Rab5 and Rab7. J. Cell Biol. 183, 513–526.
Schneider, L., Zhang, J., 2010. Lysosomal function in macromolecular homeostasis and bioenergetics in Parkinson's disease. Mol. Neurodegener. 5, 14.
Seaman, M.N., 2004. Cargo-selective endosomal sorting for retrieval to the Golgi requires retromer. J. Cell Biol. 165, 111–122.
Seaman, M.N., Marcusson, E.G., Cereghino, J.L., Emr, S.D., 1997. Endosome to Golgi retrieval of the vacuolar protein sorting receptor, Vps10p, requires the function of the VPS29, VPS30, and VPS35 gene products. J. Cell Biol. 137, 79–92.
Seaman, M.N., Harbour, M.E., Tattersall, D., Read, E., Bright, N., 2009. Membrane recruitment of the cargo-selective retromer subcomplex is catalysed by the small GTPase Rab7 and inhibited by the Rab-GAP TBC1D5. J. Cell Sci. 122, 2371–2382.
Sevlever, D., Jiang, P., Yen, S.H., 2008. Cathepsin D is the main lysosomal enzyme involved in the degradation of alpha-synuclein and generation of its carboxy-terminally truncated species. Biochemistry 47, 9678–9687.
Singleton, A.B., Farrer, M.J., Bonifati, V., 2013. The genetics of Parkinson's disease: progress and therapeutic implications. Mov. Disord. 28, 14–23.
Small, S.A., Kent, K., Pierce, A., Leung, C., Kang, M.S., Okada, H., Honig, L., Vonsattel, J.P., Kim, T. W., 2005. Model-guided microarray implicates the retromer complex in Alzheimer's disease. Ann. Neurol. 58, 909–919.
Spillantini, M.G., Schmidt, M.L., Lee, V.M., Trojanowski, J.Q., Jakes, R., Goedert, M., 1997. Alpha-synuclein in Lewy bodies. Nature 388, 839–840.
Springer, W., Kahle, P.J., 2011. Regulation of PINK1-Parkin-mediated mitophagy. Autophagy 7, 266–278.
Sugeno, N., Takeda, A., Hasegawa, T., Kobayashi, M., Kikuchi, A., Mori, F., Wakabayashi, K., Itoyama, Y., 2008. Serine 129 phosphorylation of alpha-synuclein induces unfolded protein response-mediated cell death. J. Biol. Chem. 283, 23179–23188.
Sugeno, N., Hasegawa, T., Tanaka, N., Fukuda, M., Wakabayashi, K., Oshima, R., Konno, M., Miura, E., Kikuchi, A., Baba, T., Anan, T., Nakao, M., Geisler, S., Aoki, M., Takeda, A., 2014. K63-linked ubiquitination by E3 ubiquitin ligase Nedd4-1 facilitates endosomal sequestration of internalized alpha-synuclein. J. Biol. Chem. 289, 18137–18151.
Tardiff, D.F., Jui, N.T., Khurana, V., Tambe, M.A., Thompson, M.L., Chung, C.Y., Kamadurai, H.B., Kim, H.T., Lancaster, A.K., Caldwell, K.A., Caldwell, G.A., Rochet, J.C., Buchwald, S.L., Lindquist, S., 2013. Yeast reveal a "druggable" Rsp5/Nedd4 network that ameliorates alpha-synuclein toxicity in neurons. Science 342, 979–983.
Tofaris, G.K., 2012. Lysosome-dependent pathways as a unifying theme in Parkinson's disease. Mov. Disord. 27, 1364–1369.
Tofaris, G.K., Kim, H.T., Hourez, R., Jung, J.W., Kim, K.P., Goldberg, A.L., 2011. Ubiquitin ligase Nedd4 promotes alpha-synuclein degradation by the endosomal–lysosomal pathway. Proc. Natl. Acad. Sci. U. S. A. 108, 17004–17009.
Tsakiri, E.N., Iliaki, K.K., Hohn, A., Grimm, S., Papassideri, I.S., Grune, T., Trougakos, I.P., 2013. Diet-derived advanced glycation end products or lipofuscin disrupts proteostasis and reduces life span in Drosophila melanogaster. Free Radic. Biol. Med. 65c, 1155–1163.
Tsika, E., Glauser, L., Moser, R., Fiser, A., Daniel, G., Sheerin, U.M., Lees, A., Troncoso, J.C., Lewis, P.A., Bandopadhyay, R., Schneider, B.L., Moore, D.J., 2014. Parkinson's disease-linked mutations in VPS35 induce dopaminergic neurodegeneration. Hum. Mol. Genet. 23, 4621–4638.
Vilarino-Guell, C., Wider, C., Ross, O.A., Dachsel, J.C., Kachergus, J.M., Lincoln, S.J., Soto-Ortolaza, A.I., Cobb, S.A., Wilhoite, G.J., Bacon, J.A., Behrouz, B., Melrose, H.L., Hentati, E., Puschmann, A., Evans, D.M., Conibear, E., Wasserman, W.W., Aasly, J.O., Burkhard, P.R., Djaldetti, R., Ghika, J., Hentati, F., Krygowska-Wajs, A., Lynch, T., Melamed, E., Rajput, A., Rajput, A.H., Solida, A., Wu, R.M., Uitti, R.J., Wszolek, Z.K., Vingerhoets, F., Farrer, M.J., 2011. VPS35 mutations in Parkinson disease. Am. J. Hum. Genet. 89, 162–167.
Vilarino-Guell, C., Rajput, A., Milnerwood, A.J., Shah, B., Szu-Tu, C., Trinh, J., Yu, I., Encarnacion, M., Munsie, L.N., Tapia, L., Gustavsson, E.K., Chou, P., Tatarnikov, I., Evans, D.M., Pishotta, F.T., Volta, M., Beccano-Kelly, D., Thompson, C., Lin, M.K., Sherman, H.E., Han, H.J., Guenther, B.L., Wasserman, W.W., Bernard, V., Ross, C.J., Appel-Cresswell, S., Stoessl, A.J., Robinson, C.A., Dickson, D.W., Ross, O.A., Wszolek, Z.K., Aasly, J.O., Wu, R. M., Hentati, F., Gibson, R.A., McPherson, P.S., Girard, M., Rajput, M., Rajput, A.H., Farrer, M.J., 2014. DNAJC13 mutations in Parkinson disease. Hum. Mol. Genet. 23, 1794–1801.
Vogiatzi, T., Xilouri, M., Vekrellis, K., Stefanis, L., 2008. Wild type alpha-synuclein is degraded by chaperone-mediated autophagy and macroautophagy in neuronal cells. J. Biol. Chem. 283, 23542–23556.
Wales, P., Pinho, R., Lazaro, D.F., Outeiro, T.F., 2013. Limelight on alpha-synuclein: pathological and mechanistic implications in neurodegeneration. J. Parkinsons Dis. 3, 415–459.
Wen, L., Tang, F.L., Hong, Y., Luo, S.W., Wang, C.L., He, W., Shen, C., Jung, J.U., Xiong, F., Lee, D. H., Zhang, Q.G., Brann, D., Kim, T.W., Yan, R., Mei, L., Xiong, W.C., 2011. VPS35 haploinsufficiency increases Alzheimer's disease neuropathology. J. Cell Biol. 195, 765–779.
Yamaguchi, M., Hirose, F., Inoue, Y.H., Shiraki, M., Hayashi, Y., Nishi, Y., Matsukage, A., 1999. Ectopic expression of human p53 inhibits entry into S phase and induces apoptosis in the Drosophila eye imaginal disc. Oncogene 18, 6767–6775.
Zavodszky, E., Seaman, M.N., Moreau, K., Jimenez-Sanchez, M., Breusegem, S.Y., Harbour, M. E., Rubinsztein, D.C., 2014. Mutation in VPS35 associated with Parkinson's disease impairs WASH complex association and inhibits autophagy. Nat. Commun. 5, 3828.
Zhao, X., Nothwehr, S., Lara-Lemus, R., Zhang, B.Y., Peter, H., Arvan, P., 2007. Dominant-negative behavior of mammalian Vps35 in yeast requires a conserved PRLYL motif involved in retromer assembly. Traffic 8, 1829–1840.
Zimprich, A., Benet-Pages, A., Struhal, W., Graf, E., Eck, S.H., Offman, M.N., Haubenberger, D., Spielberger, S., Schulte, E.C., Lichtner, P., Rossle, S.C., Klopp, N., Wolf, E., Seppi, K., Pirker, W., Presslauer, S., Mollenhauer, B., Katzenschlager, R., Foki, T., Hotzy, C., Reinthaler, E., Harutyunyan, A., Kralovics, R., Peters, A., Zimprich, F., Brucke, T., Poewe, W., Auff, E., Trenkwalder, C., Rost, B., Ransmayr, G., Winkelmann, J., Meitinger, T., Strom, T.M., 2011. A mutation in VPS35, encoding a subunit of the retromer complex, causes late-onset Parkinson disease. Am. J. Hum. Genet. 89, 168–175.

Neurobiology:

Lys-63-linked Ubiquitination by E3 Ubiquitin Ligase Nedd4-1 Facilitates Endosomal Sequestration of Internalized α -Synuclein

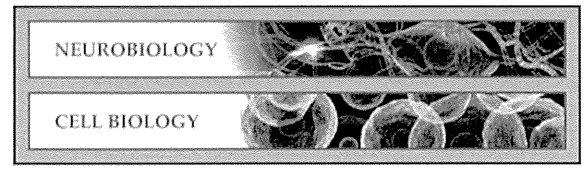

Naoto Sugeno, Takafumi Hasegawa, Nobuyuki Tanaka, Mitsunori Fukuda, Koichi Wakabayashi, Ryuji Oshima, Masashi Konno, Emiko Miura, Akio Kikuchi, Toru Baba, Tadashi Anan, Mitsuyoshi Nakao, Sven Geisler, Masashi Aoki and Atsushi Takeda

J. Biol. Chem. 2014, 289:18137-18151.
doi: 10.1074/jbc.M113.529461 originally published online May 15, 2014

THE JOURNAL OF BIOLOGICAL CHEMISTRY VOL. 289, NO. 26, pp. 18137–18151, June 27, 2014

Lys-63-linked Ubiquitination by E3 Ubiquitin Ligase Nedd4-1 Facilitates Endosomal Sequestration of Internalized α-Synuclein*

Received for publication, April 1, 2014, and in revised form, May 11, 2014 Published, JBC Papers in Press, May 15, 2014, DOI 10.1074/jbc.M113.529461

Naoto Sugeno[‡], Takafumi Hasegawa[‡1], Nobuyuki Tanaka[§], Mitsunori Fukuda[¶], Koichi Wakabayashi[‖], Ryuji Oshima[‡§], Masashi Konno[‡], Emiko Miura[‡], Akio Kikuchi[‡], Toru Baba[‡], Tadashi Anan[**], Mitsuyoshi Nakao[‡‡], Sven Geisler[§§], Masashi Aoki[‡], and Atsushi Takeda[‡2]

From the [‡]Division of Neurology, Department of Neuroscience and Sensory Organs, Tohoku University Graduate School of Medicine, Sendai 980-8574, Japan, the [§]Division of Cancer Biology and Therapeutics, Miyagi Cancer Center Research Institute, Natori 981-1293, Japan, the [¶]Laboratory of Membrane Trafficking Mechanisms, Department of Developmental Biology and Neurosciences, Graduate School of Life Sciences, Tohoku University, Sendai 980-8578, Japan, the [‖]Department of Neuropathology, Institute of Brain Science, Hirosaki University School of Medicine, Hirosaki 036-8562, Japan, the [**]Department of Pediatrics, Kumamoto University School of Medicine, Kumamoto 860-0811, Japan, the [‡‡]Department of Medical Cell Biology, Institute of Molecular Embryology and Genetics, Kumamoto University, Kumamoto 860-0811, Japan, and the [§§]Laboratory of Functional Neurogenetics, Department for Neurodegenerative Diseases, Hertie Institute for Clinical Brain Research, University of Tübingen, German Centre for Neurodegenerative Diseases, Tübingen 72076, Germany

Background: Nedd4-1 catalyzes the Lys-63-linked ubiquitination of aS.
Results: The Lys-63-linked ubiquitination of aS by Nedd4-1 facilitates endosomal targeting of extracellular aS.
Conclusion: Compared with C-terminal deficient mutants, wild type-aS is preferentially internalized and translocates to endosomes. The overexpression of Nedd4-1 leads to the accumulation of aS in endosomes.
Significance: Nedd4-1-mediated Lys-63 ubiquitination specifies the fate of internalized aS.

α-Synuclein (aS) is a major constituent of Lewy bodies, which are not only a pathological marker for Parkinson disease but also a trigger for neurodegeneration. Cumulative evidence suggests that aS spreads from cell to cell and thereby propagates neurodegeneration to neighboring cells. Recently, Nedd4-1 (neural precursor cell expressed developmentally down-regulated protein 4-1), an E3 ubiquitin ligase, was shown to catalyze the Lys-63-linked polyubiquitination of intracellular aS and thereby facilitate aS degradation by the endolysosomal pathway. Because Nedd4-1 exerts its activity in close proximity to the inner leaflet of the plasma membrane, we speculate that after the internalization of aS the membrane resident aS is preferentially ubiquitinated by Nedd4-1. To clarify the role of Nedd4-1 in aS internalization and endolysosomal sequestration, we generated aS mutants, including ΔPR1(1–119 and 129–140), ΔC(1–119), and ΔPR2(1–119 and 134–140), that lack the proline-rich sequence, a putative Nedd4-1 recognition site. We show that wild type aS, but not ΔPR1, ΔPR2, or ΔC aS, is modified by Nedd4-1 *in vitro*, acquiring a Lys-63-linked ubiquitin chain. Compared with the mutants lacking the proline-rich sequence, wild type-aS is preferentially internalized and translocated to endosomes. The overexpression of Nedd4-1 increased aS in endosomes, whereas RNAi-mediated silencing of Nedd4-1 decreased endosomal aS. Although aS freely passes through plasma membranes within minutes, a pulse-chase experiment revealed that the overexpression of Nedd4-1 markedly decreased the re-secretion of internalized aS. Together, these findings demonstrate that Nedd4-1-linked Lys-63 ubiquitination specifies the fate of extrinsic and *de novo* synthesized aS by facilitating their targeting to endosomes.

The intraneuronal aggregation of misfolded α-synuclein (aS),[3] known as a component of Lewy bodies (LB), is a pathological hallmark of Parkinson disease (PD). After the discovery of LB-like inclusions in the grafted neurons of PD patients who had previously received transplants of fetal mesencephalic neurons (1), increasing evidence has suggested that both monomeric and oligomeric aS can be secreted into the extracellular milieu (2), thereby affecting the physiological state of neighboring cells. Previous studies have revealed that the cellular uptake of fibrillar aS requires physiological temperatures and dynamin-1 (3, 4), a master regulator of endocytic vesicle formation, suggesting the

* This work was supported in part by Grants-in-aid for Scientific Research (C) 25461264 and 23591228, Grant-in-aid for Scientific Research (B) 24390219, Grant-in-aid for Exploratory Research 24659423, Grant-in-aid for Scientific Research on Innovative Areas (Brain Environment) 24111502 from the Ministry of Education, Culture, Sports, Science and Technology, a grant from the Research Committee for Ataxic Diseases, the Ministry of Health, Labor, and Welfare, Japan, a grant from the Symposium on Catecholamine and Neurological Disorders, and a grant from the 17th Takeda Science Foundation Symposium on Bioscience.
[1] To whom correspondence should be addressed. Tel.: 81-22-717-7189; Fax: 81-22-717-7192; E-mail: thasegawa@med.tohoku.ac.jp.
[2] Present address: Dept. of Neurology, National Hospital Organization, Sendai-Nishitaga Hospital, Sendai 982-8555, Japan.

[3] The abbreviations used are: aS, α-synuclein; CQ, chloroquine; HECT, homologous to the E6-AP C terminus; HMW, high molecular weight; LB, Lewy body; LMW, low molecular weight; Nedd4, neural precursor cell expressed developmentally down-regulated protein 4; pAb, polyclonal antibody; PD, Parkinson disease; PR, proline-rich; aS, α-synuclein; Tricine, *N*-[2-hydroxy-1,1-bis(hydroxymethyl)ethyl]glycine; ESCRT, endosomal sorting complex required for transport; BN, blue native.